Adjoint sensitivity analysis of regional air quality models

Adrian Sandu [a,*], Dacian N. Daescu [b], Gregory R. Carmichael [c,1], Tianfeng Chai [c,1]

[a] *Department of Computer Science, Virginia Polytechnic Institute and State University, 660 McBryde Hall, Blacksburg, VA 24061, USA*
[b] *Department of Mathematics and Statistics, Portland State University, Portland, OR 97207-0751, USA*
[c] *Center for Global and Regional Environmental Research, 204 IATL, The University of Iowa, Iowa City, IA 52242-1297, USA*

Abstract

The task of providing an optimal analysis of the state of the atmosphere requires the development of efficient computational tools that facilitate an efficient integration of observational data into models. In a variational approach the data assimilation problem is posed as a minimization problem, which requires the sensitivity (derivatives) of a cost functional with respect to problem parameters. The direct decoupled method has been extensively applied for sensitivity studies of air pollution. Adjoint sensitivity is a complementary approach which efficiently calculates the derivatives of a functional with respect to a large number of parameters. In this paper, we discuss the mathematical foundations of the adjoint sensitivity method applied to air pollution models, and present a complete set of computational tools for performing three-dimensional adjoint sensitivity studies. Numerical examples show that three-dimensional adjoint sensitivity analysis provides information on influence areas, which cannot be obtained solely by an inverse analysis of the meteorological fields. Several illustrative data assimilation results in a twin experiments framework, as well as the assimilation of a real data set are also presented.
© 2004 Published by Elsevier Inc.

Keywords: Chemical transport models; Adjoint models; Sensitivity analysis; Data assimilation

1. Introduction

Our ability to anticipate and manage changes in atmospheric pollutant concentrations relies on an accurate representation of the chemical state of the atmosphere. As our fundamental understanding of

---

* Corresponding author. Tel.: +1 540 231 2193; fax: +1 540 231 6075.
E-mail addresses: asandu@cs.vt.edu (A. Sandu), daescu@pdx.edu (D.N. Daescu), gcarmich@cgrer.uiowa.edu (G.R. Carmichael), tchai@cgrer.uiowa.edu (T. Chai).
[1] Tel.: +1 319 335 3333; fax: +1 319 335 3337.

atmospheric chemistry advances, novel computational tools are needed to integrate observational data and models together to provide the best, physically consistent estimate of the evolving chemical state of the atmosphere. Such an analysis state better defines the spatial and temporal fields of key chemical components in relation to their sources and sinks. This information is critical in designing cost-effective emission control strategies for improved air quality, for the interpretation of observational data such as those obtained during intensive field campaigns, and to the execution of air-quality forecasting.

Kalman filter techniques [31] provide a stochastic approach to the data assimilation problem. The filtering theory is described in Jazwinski [30] and the applicability to atmospheric modeling is presented in the work of Daley [34]. A Kalman filter approach was used by Menard et al. [38] to assimilate methane observations into a stratospheric tracer model. The computational burden associated to the filtering process has prevented the implementation of the full Kalman filter for large-scale transport-chemistry models. Ensemble Kalman filter techniques [20,27] may be used to facilitate the practical implementation as shown by van Loon et al. [48].

Variational methods (3D-Var, 4D-Var) provide an optimal control approach to the data assimilation problem. Four-dimensional variational (4D-Var) data assimilation allows the optimal combination of three sources of information: an a priori (background) estimate of the state of the atmosphere; knowledge about the physical and chemical processes that govern the evolution of pollutant fields, as captured in the model (CTM); and observations of some of the state variables. The optimal analysis state is obtained through a minimization process to provide the best fit to the background estimate and to all observational data (space and time distributed) available in the assimilation window. The use of adjoint modeling to evaluate the gradient of the objective functional makes feasible the implementation of the 4D-Var data assimilation for large-scale atmospheric models. The practical applicability of the 4D-Var typically requires an accurate model representation of the atmospheric dynamics. Under the perfect model assumption and with valid covariance matrices, the Hessian of the minimized cost function equals the inverse of the covariance matrix of the analysis error. The optimality of the 4D-Var and its relationship with the Kalman filter is further discussed in [35].

The direct decoupled method has been extensively used for sensitivity studies in three dimensional (3D) atmospheric chemistry transport simulations [25,51,52]. Direct sensitivity analysis via (forward mode) automatic differentiation was also employed in the context of photochemical transport models [5,26,29]. Adjoint sensitivity is a complementary approach which efficiently calculates the derivatives of a functional with respect to a large number of parameters.

In this paper, we present the mathematical theory of adjoint sensitivity analysis applied to three dimensional atmospheric transport and chemistry models. We discuss the computational tools developed and use them to build the adjoint of a comprehensive 3D air quality model. This discussion includes parallelization and performance of 3D adjoints. The use of adjoints for sensitivity analysis and for data assimilation problems is illustrated using numerical simulations of air pollution in East Asia.

The paper is organized as follows. Section 2 gives an overview of previous work in chemical data assimilation. In Section 3, we review the mathematical theory of adjoint sensitivity analysis applied to air quality modeling. Specific algorithmic details of the adjoint of Stem-III chemical transport model are presented in Section 4, while Section 5 discusses implementation aspects. Numerical results for the simulation of East Asia are shown in Section 6. Conclusions and future research directions are given in Section 7.

2. Previous 4D-Var work

The implementation of the four-dimensional variational (4D-Var) data assimilation for large-scale atmospheric models relies on the adjoint modeling to provide the gradient of the objective functional. Mathematical foundations of the adjoint sensitivity for nonlinear dynamical systems are presented by Cacuci

[3,4] and Marchuk et al. [36,37]. Early applications of the 4D-Var to chemical data assimilation were presented by Fisher and Lary [21] for a stratospheric photochemical box model with trajectories. A similar model was used later by Khattatov et al. [32] to implement both the 4D-Var and a Kalman filter method. A tropospheric gas-phase box model based on the chemical mechanism RADM2 was used by Elbern et al. [16] to analyze the applicability of the 4D-Var approach to tropospheric chemical data assimilation. Menut et al. [33] and Vautard et al. [47] use the adjoint approach for sensitivity studies in atmospheric chemistry modeling.

In the past few years variational methods have been successfully used in data assimilation for comprehensive three-dimensional atmospheric chemistry models [14,19]. The work of Wang et al. [50] provides a review of the adjoint methodology and data assimilation applications to atmospheric chemistry.

The inverse problem of data assimilation of tropospheric gas observations into a comprehensive 3-dimensional Eulerian CTM is researched by Elbern et al. [14]. The authors use the discrete parallel adjoint of the European Air Pollution Dispersion Model EURAD-CTM2 with RADM2 gas phase chemical mechanism. An operator split approach, with Bott's advection scheme and QSSA chemical solver is used. The implementations aspects are discussed in [17]. The 4D-Var method is always able to retrieve the concentrations of observed species. It is concluded that the relative scaling of different species (which amounts to a preconditioning of the minimization problem) is important and impacts the assimilation skills.

Elbern et al. [18] study the skill and limits of 4D-Var techniques to analyze the emission rates of precursor constituents of ozone, with only ozone observations available. They conclude that NO_x emissions could be successfully analyzed for their strength, while for individual VOC emissions regularization techniques are needed to account for known ratios of individual species.

Improvements in ozone prediction through the assimilation of observations are considered by Elbern et al. [15]. Observations of chemical constituents were used from the EMEP database, and national, regional, and urban surface observations across Europe. Marked improvements after the assimilation of ozone measurements are noticed.

Other techniques available for data assimilation have been successfully applied to atmospheric chemistry models. For example, van Loon et al. [48] used an ensemble Kalman filter approach to assimilate ground level ozone measurements and improve uncertainties in the emission rates of NO_x, SO_x, VOC and CO in Europe.

3. Mathematical considerations

In this section a review of the mathematical aspects of chemical transport modeling and adjoint sensitivity analysis is presented. Both the continuous and discrete adjoint approaches are described (see also Wang et al. [50]).

3.1. Atmospheric chemistry and transport modeling

In what follows we denote by u the wind field vector, K the turbulent diffusivity tensor, ρ the air density in moles/cm^3, and c_i the mole-fraction concentration of chemical species i ($1 \leqslant i \leqslant s$). The density of this species is ρc_i moles/cm^3. Let V_i^{dep} be the deposition velocity of species i, Q_i the rate of surface emissions, and E_i the rate of elevated emissions for this species. The rate of chemical transformations f_i depends on absolute concentration values; the rate at which mole-fraction concentrations change is then $f_i(\rho c)/\rho$.

Consider a domain Ω which covers a region of the atmosphere. Let $\boldsymbol{n}$ be the outward normal vector on each point of the boundary $\partial\Omega$. At each time moment the boundary of the domain is partitioned into $\partial\Omega = \Gamma^{\text{IN}} \cup \Gamma^{\text{OUT}} \cup \Gamma^{\text{GR}}$ where Γ^{GR} is the ground level portion of the boundary; Γ^{IN} is the set of (lateral or top) boundary points where $u \cdot \boldsymbol{n} \leqslant 0$ and Γ^{OUT} the set where $u \cdot \boldsymbol{n} > 0$.

The evolution of concentrations in time is described by the material balance equations

$$\frac{\partial c_i}{\partial t} = -u \cdot \nabla c_i + \frac{1}{\rho} \nabla \cdot (\rho K \nabla c_i) + \frac{1}{\rho} f_i(\rho c) + E_i, \quad t^0 \leqslant t \leqslant T, \tag{1a}$$

$$c_i(t^0, x) = c_i^0(x), \tag{1b}$$

$$c_i(t, x) = c_i^{\text{IN}}(t, x) \quad \text{for } x \in \Gamma^{\text{IN}}, \tag{1c}$$

$$K \frac{\partial c_i}{\partial n} = 0 \quad \text{for } x \in \Gamma^{\text{OUT}}, \tag{1d}$$

$$K \frac{\partial c_i}{\partial n} = V_i^{\text{dep}} c_i - Q_i \quad \text{for } x \in \Gamma^{\text{GR}}, \quad \text{for all } 1 \leqslant i \leqslant s. \tag{1e}$$

We refer to the system (1a)–(1e) as the *forward (direct) model*. To simplify the presentation, in this paper we consider as parameters the initial state c^0 of the model; it is known that this does not restrict the generality of the formulation. The solution of the forward model $c = c(t, c^0)$ is uniquely determined once the model parameters c^0 are specified.

The direct model (1a)–(1e) is solved by a sequence of N timesteps of length Δt taken between t^0 and $t^N = T$. At each time step one calculates the numerical approximation $c^k(x) \approx c(t^k, x)$ at $t^k = t^0 + k\Delta t$ such that

$$c^{k+1} = \mathcal{N}_{[t^k, t^{k+1}]} \circ c^k, \quad c^N = \prod_{k=0}^{N-1} \mathcal{N}_{[t^k, t^{k+1}]} \circ c^0. \tag{2}$$

The numerical solution operator $\mathcal{N}$ is based on an operator splitting approach, where the transport steps along each direction and the chemistry steps are taken successively. Operator splitting is standard practice in computational air pollution modeling [24]. It allows the development of the forward, tangent linear, and adjoint models with relative ease. Formally, if we denote by $\mathcal{T}$ the numerical solution operator for directional transport, and by $\mathcal{C}$ the solution operator for chemistry we have

$$\mathcal{N}_{[t, t+\Delta t]} = \mathcal{T}_X^{\Delta t/2} \circ \mathcal{T}_Y^{\Delta t/2} \circ \mathcal{T}_Z^{\Delta t/2} \circ \mathcal{C}^{\Delta t} \circ \mathcal{T}_Z^{\Delta t/2} \circ \mathcal{T}_Y^{\Delta t/2} \circ \mathcal{T}_X^{\Delta t/2}. \tag{3}$$

The numerical errors introduced by splitting are an important component of model errors (see e.g., [46]). In this paper, for the purpose of 4D-Var data assimilation, we assume the model errors to be small. Indeed, in computational air pollution modeling the splitting errors oscillate with the diurnal cycle and do not grow unboundedly for evolving time [24].

An infinitesimal perturbation δc^0 in the parameters will result in perturbations $\delta c_i(t)$ of the concentration fields. These perturbations are solutions of the *tangent linear model* as discussed in Appendix A. In the direct sensitivity analysis approach one solves the model (1a)–(1e) together with the tangent linear model forward in time [51].

3.2. Continuous adjoint sensitivity analysis

Consider a scalar response functional defined in terms of the model solution $c(t)$

$$\mathcal{J}(c^0) = \int_{t^0}^{T} \int_{\Omega} g(c(t, x)) \, dx \, dt. \tag{4}$$

The response depends implicitly on the parameters c^0 via the dependence of $c(t)$ on c^0. The continuous adjoint model is defined as the adjoint of the tangent linear model as explained in Appendix A. By imposing the Lagrange identity and after a careful integration by parts [10,36] one arrives at the following equations that govern the evolution of the adjoint variables:

$$\frac{\partial \lambda_i}{\partial t} = -\nabla \cdot (u\lambda_i) - \nabla \cdot \left(\rho K \nabla \frac{\lambda_i}{\rho} \right) - \left(F^T(\rho c)\lambda \right)_i - \phi_i, \quad T \geqslant t \geqslant t^0, \tag{5a}$$

$$\lambda_i(T,x) = \lambda_i^F(x), \tag{5b}$$

$$\lambda_i(t,x) = 0 \quad \text{for } x \in \Gamma^{\text{IN}}, \tag{5c}$$

$$\lambda_i u + \rho K \frac{\partial(\lambda_i/\rho)}{\partial n} = 0 \quad \text{for } x \in \Gamma^{\text{OUT}}, \tag{5d}$$

$$\rho K \frac{\partial(\lambda_i/\rho)}{\partial n} = V_i^{\text{dep}} \lambda_i \quad \text{for } x \in \Gamma^{\text{GR}}, \quad \text{for all } 1 \leqslant i \leqslant s, \tag{5e}$$

where

$$\phi_i(t,x) = \frac{\partial g(c_1, \dots, c_n)}{\partial c_i}(t,x), \quad \lambda_i^F(x) = 0, \tag{6}$$

and $\lambda_i(t,x)$ are the adjoint variables associated with the concentrations $c_i(t,x)$, $1 \leqslant i \leqslant s$. In the above $F = \partial f / \partial c$ is the Jacobian of the chemical rate function f. A typical sparsity structure for the Jacobians of atmospheric chemistry is shown in Fig. 1. A detailed discussion of the chemical terms in the context of adjoint modeling can be found in [9,42]. To obtain the ground boundary condition we use the fact that $u \cdot n = 0$ at ground level. We refer to (5a)–(5e) as the *(continuous) adjoint system* of the tangent linear model. The adjoint variables $\lambda(t,x)$ are also called *influence functions* [1] and represent the sensitivies of the response functional to perturbations in the state variables $c(t,x)$

$$\lambda_i(t,x) = \frac{\partial \mathscr{J}}{\partial c_i(t,x)}. \tag{7}$$
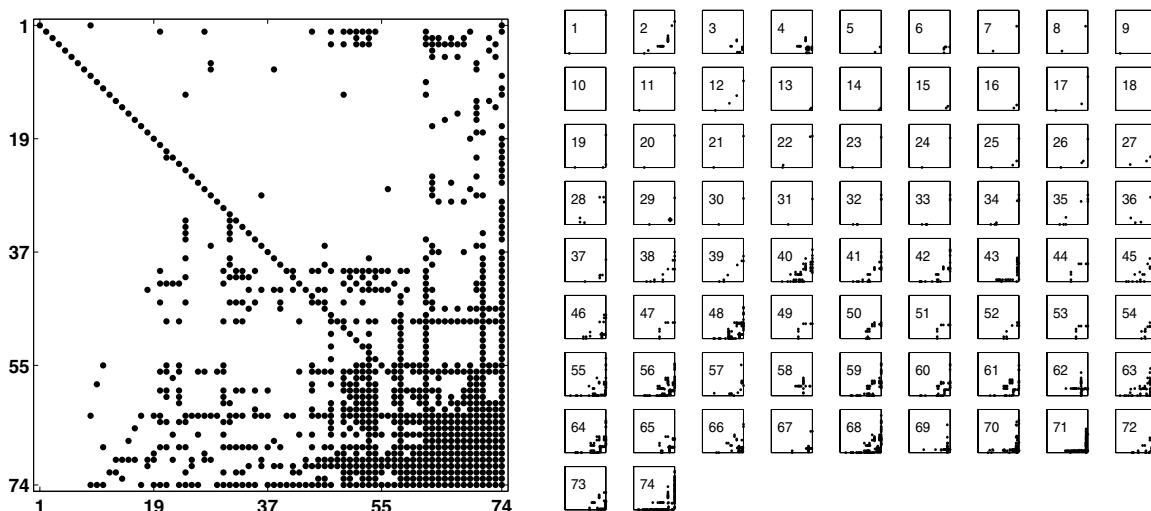

Fig. 1. Left panel: sparsity structure of the SAPRC-99 Jacobian (with fill-in). There are 920 nonzero entries out of 5476, i.e. the sparsity is about 17%. Right panel: sparsity structure of the SAPRC-99 Hessian (represented as one Hessian matrix per component). There are 1696 nonzero entries, i.e. the sparsity is about 0.4%.

In the context of optimal control where the minimization of the functional (4) is required, the adjoint variables may be also interpreted as Lagrange multipliers by imposing the forward model equations as strong constraints (see Appendix A).

The adjoint system (5a)–(5e) depends on the state of the forward model (i.e. on the concentration fields $c(t,x)$) through the nonlinear chemical term $F(\rho c)$ and possibly through the forcing term ϕ for nonlinear functionals. Note that the adjoint initial condition is posed at the final time T such that the forward model must be first solved forward in time, the state $c(x,t)$ saved for all t, then the adjoint model could be integrated backwards in time from T down to t^0.

In practice a hybrid approach is used. The forward model is solved using a numerical method, and the numerical approximation of the state is saved periodically. These checkpoints are used in the definition of the adjoint equations. The continuous adjoint equation (5a)–(5e) is a convection-diffusion-reaction equation (with linearized chemistry) and can be solved by any numerical method of choice. In particular an operator splitting approach could be employed using the same numerical methods as for solving the direct model

$$\lambda^k = \mathcal{N}_{[t^{k+1},t^k]} \circ \lambda^{k+1}, \quad \lambda^0 = \prod_{k=0}^{N-1} \mathcal{N}_{[t^{N-k},t^{N-k-1}]} \circ \lambda^N. \tag{8}$$

For different cost functionals the forcing ϕ_i and the initial values λ_i^F are chosen such that the adjoint variables are the sensitivities of the cost functional (7). We now discuss some examples relevant in applications.

Example 1. In many practical situations the cost functional is not integral in time, but is evaluated at a set of discrete time moments $\{t^k\}_{0 \leqslant k \leqslant N}$, which usually contain the endpoints t^0 and $t^N = T$.

$$\mathcal{J}(c^0) = \sum_{k=0}^{N} \int_{\Omega} g_k\big(c(t^k,x)\big)\mathrm{d}x. \tag{9}$$

The forcing factor ϕ_i in the adjoint will contain delta functions at measurement times Δ_{t-t^k}. An equivalent formulation is to divide the integration interval into subintervals

$$\mathcal{I}^k = \big[t^k, t^{k+1}\big). \tag{10}$$

On each subinterval $\mathcal{I}^k$ the backward adjoint integration is carried out using

$$\phi_i = 0, \quad \lambda_i(t^{k+1} - \epsilon, x) = \lambda_i(t^{k+1} + \epsilon, x) + \frac{\partial g_{k+1}(c_1,\dots,c_n)}{\partial c_i}(t^{k+1},x), \quad \epsilon \to 0. \tag{11}$$

In other words, the initial adjoint value in one interval is obtained from the final adjoint value in the next time interval, plus a jump given by the derivative of the observation function. For the final interval $k = N - 1$ we use the convention that $\lambda_i(t^F + \epsilon, x) = 0$.

Example 2. If the functional is defined using only solution values at selected points $\{x_j^*\}_j$ in the domain (for example at measurement sites)

$$\mathcal{J}(c^0) = \int_{t^0}^{T} \sum_j g_j\big(c(t,x_j^*)\big)\mathrm{d}t, \tag{12}$$

then

$$\phi_i(t,x) = \sum_j \frac{\partial g_j(c_1,\dots,c_n)}{\partial c_i}(t,x_j^*)\delta_{x-x_j^*}, \quad \lambda_i^F(x) = 0. \tag{13}$$

3.3. Discrete adjoint sensitivity analysis

In this approach the numerical discretization (2) of the (1a)–(1e) is considered to be the forward model. This is a pragmatic view, as only the numerical model is in fact available for analysis. For brevity the state of the discretized model will be denoted $c_i^k[j]$, where i is the species index, j is the space discretization index and k the time discretization index. $c^k[j]$ will refer to the vector of all species at time level k and grid level j. The cost functional is defined in terms of the discrete model state

$$\mathscr{I}(c^0) = \sum_{k=0}^{N} \sum_{j} g(c^k[j]),$$

(14)

and one wants the derivatives of this functional with respect to the discrete model parameters $c_i^0[j]$. A perturbation δc^0 in the parameters c^0 propagates in time according to the tangent linear discrete equation

$$\delta c^{k+1} = \mathscr{N}'_{[t^k,t^{k+1}]} \circ \delta c^k, \quad \delta c^N = \prod_{i=0}^{N-1} \mathscr{N}'_{[t^k,t^{k+1}]} \circ \delta c^0,$$

(15)

where $\mathscr{N}'$ is the tangent linear operator associated with the solution operator $\mathscr{N}$. For an operator splitting approach (3) $\mathscr{N}'$ is built from the tangent linear transport and chemistry operators

$$\mathscr{N}'_{[t,t+\Delta t]} = \mathscr{T}'^{\Delta t/2}_X \circ \mathscr{T}'^{\Delta t/2}_Y \circ \mathscr{T}'^{\Delta t/2}_Z \circ \mathscr{C}'^{\Delta t} \circ \mathscr{T}'^{\Delta t/2}_Z \circ \mathscr{T}'^{\Delta t/2}_Y \circ \mathscr{T}'^{\Delta t/2}_X.$$

(16)

To each tangent linear operator corresponds an adjoint operator (denoted here with a star superscript). The adjoint equation of (16) is

$$\mathscr{N}'^{*}_{[t+\Delta t,t]} = \mathscr{T}'^{*\Delta t/2}_X \circ \mathscr{T}'^{*\Delta t/2}_Y \circ \mathscr{T}'^{*\Delta t/2}_Z \circ \mathscr{C}'^{*\Delta t} \circ \mathscr{T}'^{*\Delta t/2}_Z \circ \mathscr{T}'^{*\Delta t/2}_Y \circ \mathscr{T}'^{*\Delta t/2}_X,$$

(17)

such that the resulting *(discrete) adjoint model* is

$$\lambda^k = \mathscr{N}'^{*}_{[t^{k+1},t^k]} \circ \lambda^{k+1} + \phi^k, \quad k = N-1, N-2, \ldots 0; \quad \lambda^N[j] = \lambda^F(x_j).$$

(18)

The forcing function ϕ and the initial values λ^N are chosen such that the adjoint variables are sensitivities of the functional with respect to the state variables

$$\lambda_i^k[j] = \frac{\partial \mathscr{I}(c^0)}{\partial c_i^k[j]}.$$

(19)

Example 3. For the functional (14)

$$\phi_i^k[j] = \frac{\partial g}{\partial c_i}(c^k[j]), \quad \lambda_i^N[j] = \frac{\partial g}{\partial c_i}(c^N[j]).$$

(20)

Example 4. For data assimilation applications, let us assume the availability of observations $c^{k,\mathrm{obs}}$ of the state variables c^k. The cost functional measures the distance between model output and observations, as well as the deviation of the solution from the background state.

$$\mathscr{I}(c^0) = \frac{1}{2}(c^0 - c^b)^{\mathrm{T}} B^{-1}(c^0 - c^b) + \frac{1}{2} \sum_{k=1}^{N} (c^k - c^{k,\mathrm{obs}})^{\mathrm{T}} R_k^{-1}(c^k - c^{k,\mathrm{obs}}).$$

(21)

In the above the covariance matrix R^{-1} accounts for observation and representativeness errors. c^b is the background concentration (the initial guess in the assimilation procedure) and B the covariance matrix

of the estimated background error. The covariance matrices account for error correlations between different species as well as different locations. The discrete adjoint model (18) is then completely specified with

$$\phi^k = R_k^{-1}\left(c^k - c^{k,\text{obs}}\right) \quad \text{for } k \geqslant 1, \quad \lambda^N = R_N^{-1}\left(c^N - c^{N,\text{obs}}\right), \quad \frac{\partial \mathscr{J}(c^0)}{\partial c^0} = \lambda^0 + B^{-1}\left(c^0 - c^b\right), \tag{22}$$

The last relation reflects the influence of the background term on the gradient.

3.4. Comments

The direct decoupled method has been extensively used for sensitivity studies in three dimensional (3D) atmospheric chemistry transport simulations [12,13,25,51,52]. Direct sensitivity analysis via (forward mode) automatic differentiation has also been employed in the context of photochemical transport models [5,26,29]. The direct decoupled method works well for a small number of parameters. The adjoint method is a complementary approach, which works efficiently for a small number of target functions (e.g. a single functional) and a large number of parameters (e.g. the discrete initial state), as needed in the context of data assimilation.

In the adjoint sensitivity analysis one distinguishes between the continuous and the discrete adjoint modeling, see Sirkes and Tziperman [45]. Continuous adjoint sensitivity in practice is solved numerically, resulting in a discretization of the continuous adjoint equations. On the other hand the discrete adjoints are computed from the adjoint of the numerical discretization. The operations of discretization and adjoint usually do not commute, i.e. the discrete and the continuous adjoint approaches lead to different results.

The consistency of discrete adjoints with the continuous adjoint equation is a topic of ongoing research. Sei and Symes [44] analyzed several simple discretization schemes for the one dimensional nonlinear advection equation and concluded that consistency of discrete adjoints is not automatic. Sirkes and Tziperman [45] studied a one-dimensional convection-diffusion equation solved using central differences for both advection and diffusion and leap-frog time stepping. They showed that the discrete adjoint leads to strong oscillatory numerical artifacts. For time integration algorithms, Hager [22] gave order conditions for the discrete adjoints of Runge–Kutta methods to be consistent discretizations of the continuous adjoint equations. The linear stability region of the discrete adjoint coincides with the stability region of the forward method. For example, the Crank–Nicholson time discretization used in STEM (Section 4) is a second order Runge–Kutta scheme; its adjoint is a second order discretization of the continuous adjoint equations.

The discrete adjoints are in principle preferred for (smooth) data assimilation problems since they provide the exact derivative of the discrete function being minimized. They are also necessary in the computation of total energy or Hessian singular vectors. A hybrid adjoint model approach (discrete adjoint for the transport integration, continuous adjoint for the chemistry integration) was successfully applied to 4D-Var chemical data assimilation by Errera and Fonteyn [19]. For sensitivity studies using the adjoint method one wants to approximate the sensitivities of the continuous model, i.e. in this case a continuous adjoint approach may be preferable.

4. Numerical aspects of adjoint STEM-III

We now describe the construction of the adjoint of the comprehensive chemical transport model STEM-III. The forward model is solved using an operator splitting approach. The resulting discrete adjoint sensitivity model is also split. We discuss in detail the numerical techniques used for the solution of the forward model and the resulting discrete adjoints. For simplicity we use linear finite difference discretizations of the transport terms. Typical finite volume discretizations with flux limiting can be applied to the conservative

form of the mass balance equations and result in nonlinear semidiscrete transport equations. The action of the limiter is discontinuous with respect to the solution. This may lead to considerable theoretical and practical difficulties in the construction of the discrete adjoints, as well as in the understanding of their properties (see e.g., Homescu and Navon [23]). While we recognize that the study of discrete adjoints for flux limited methods is an important area of ongoing research, the current focus on simple linear (with respect to the solution) discretizations of the transport terms should be regarded as a first step toward robust data assimilation systems for air quality.

4.1. Horizontal transport

Horizontal transport is solved using a directional x and y split approach. The basic numerical techniques solve the one-dimensional transport equation

$$\frac{\partial c}{\partial t} = -u\frac{\partial c}{\partial x} + \frac{1}{\rho}\frac{\partial}{\partial x}\left(\rho K\frac{\partial c}{\partial x}\right), \quad c(t, x_{in}) = c_{in}(t), \quad K\frac{\partial c}{\partial x}\bigg|_{x_{out}} = 0. \tag{23}$$

The horizontal advection term is discretized by the third order upwind finite difference formula [28]

$$-\left(u\frac{\partial c}{\partial x}\right)\bigg|_{x=x_i} = \begin{cases} u_i(-c_{i-2} + 6c_{i-1} - 3c_i - 2c_{i+1})/(6\Delta x), & \text{if } u_i \geqslant 0, \\ u_i(2c_{i-1} + 3c_i - 6c_{i+1} + c_{i+2})/(6\Delta x), & \text{if } u_i < 0. \end{cases} \tag{24}$$

The diffusion terms are discretized by the second order central differences

$$\frac{1}{\rho}\frac{\partial}{\partial x}\left(\rho K\frac{\partial c}{\partial x}\right)\bigg|_{x=x_i} = \frac{(\rho_{i+1}K_{i+1} + \rho_i K_i)(c_{i+1} - c_i) - (\rho_i K_i + \rho_{i-1}K_{i-1})(c_i - c_{i-1})}{2\rho_i \Delta x^2}. \tag{25}$$

For the inflow boundary the advection discretization drops to the first order upwind scheme, which makes the order of consistency of the whole scheme quadratic for the interior points of the domain. If $u_1 \geqslant 0$ then x_1 is an inflow boundary point; let c_{in} be the corresponding boundary concentration (Dirichlet condition). The discretization reads

$$\frac{dc_1}{dt} = -u_1\frac{c_1 - c_{in}}{\Delta x} + \frac{(\rho_2 K_2 + \rho_1 K_1)(c_2 - c_1) - (3\rho_1 K_1 - \rho_2 K_2)(c_1 - c_{in})}{2\rho_1 \Delta x^2}. \tag{26}$$

For the outflow boundary the advection discretization also drops to the first order upwind scheme. If $u_N \geqslant 0$ then x_N is an outflow boundary point; we use the boundary condition of zero diffusive flux across the outflow boundary. The discretization reads

$$\frac{dc_N}{dt} = -u_N\frac{c_N - c_{N-1}}{\Delta x} + \frac{-(\rho_N K_N + \rho_{N-1}K_{N-1})(c_N - c_{N-1})}{2\rho_N \Delta x^2}. \tag{27}$$

The space semi-discretization leads to the linear ordinary differential equation

$$\frac{dc}{dt} = A(t)c(t) + B(t), \tag{28}$$

where the matrix $A(t)$ depends on the wind field, the diffusion tensor, and the air density but it does not depend on the unknown concentrations (for the discretization schemes under consideration). The vector B(t) represents the Dirichlet boundary conditions.

The forward system is advanced in time from t^n to $t^{n+1} = t^n + \Delta t$ using Crank–Nicholson

$$c^{n+1} = \left(I - \frac{\Delta t}{2}A(t^{n+1})\right)^{-1}\left[\left(I + \frac{\Delta t}{2}A(t^n)\right)c^n + \Delta t\frac{B(t^n) + B(t^{n+1})}{2}\right]. \tag{29}$$

The chosen discretization leads to pentadiagonal matrices and systems which can be solved very efficiently.

Eq. (29) represents the forward discrete model for horizontal transport. The corresponding adjoint system is then advanced backwards in time using the discrete adjoint formulation

$$\lambda^n = \left(I + \frac{\Delta t}{2} A^{\mathrm{T}}(t^n)\right)\left(I - \frac{\Delta t}{2} A^{\mathrm{T}}(t^{n+1})\right)^{-1} \lambda^{n+1}. \tag{30}$$

Eq. (30) is a consistent time discretization of the continuous adjoint equation. Note that for time dependent coefficient matrix the continuous adjoint discretized with Crank–Nicholson

$$\lambda^n = \left(I - \frac{\Delta t}{2} A^{\mathrm{T}}(t^n)\right)^{-1}\left(I + \frac{\Delta t}{2} A^{\mathrm{T}}(t^{n+1})\right) \lambda^{n+1}, \tag{31}$$

it is different than the discrete formula (30).

4.2. Vertical transport

The vertical advection term is discretized by the first order upwind finite difference formula

$$-\left(w \frac{\partial c}{\partial z}\right)\bigg|_{z=z_i} = \begin{cases} -w_i(c_i - c_{i-1})/(z_i - z_{i-1}), & \text{if } w_i \geqslant 0, \\ -w_i(c_{i+1} - c_i)/(z_{i+1} - z_i), & \text{if } w_i < 0. \end{cases} \tag{32}$$

The vertical diffusion is discretized by the second order central differences. Note that the vertical grid is not uniform. The top boundary condition is Dirichlet for inflow and Neumann for outflow (i.e. zero diffusive flux through the top outflow boundary). This is similar to the horizontal advection case.

The ground level boundary condition considers the flow of material given by surface emission rates Q and by deposition processes with deposition velocity V. The vertical wind speed at ground level is $w_1 = 0$. The ground boundary condition reads

$$-K \frac{\partial c}{\partial z}\bigg|_{z=\text{ground}} = Q - Vc, \tag{33}$$

where K is the vertical eddy diffusivity.

The ground level concentration is discretized in space as

$$c_1' = \frac{(\rho_2 K_2 + \rho_1 K_1)(c_2 - c_1)}{2\rho_1(z_2 - z_1)\Delta z_1} - \frac{Vc_1 - Q}{\Delta z_1}, \tag{34}$$

where Δz_1 is the height of the first layer.

This space semi-discretization leads to the linear ODE

$$c'(t) = A(t)c(t) + B(t)e_N + \frac{Q(t)}{\Delta z_1} e_1, \tag{35}$$

where the entry $A_{1,1}$ accounts now also for the deposition velocity; B accounts for the top boundary and Q accounts for ground emissions. Here e_j is the jth column of the identity matrix.

Using Crank–Nicholson time stepping for the concentrations and forward Euler timestepping for the boundaries and the ground emissions the forward discrete model for vertical transport reads

$$c^{n+1} = \left(I - \frac{\Delta t}{2} A(t^{n+1})\right)^{-1}\left[\left(I + \frac{\Delta t}{2} A(t^n)\right)c^n + \Delta t\left(B(t^n)e_N + \frac{Q(t^n)}{\Delta z_1} e_1\right)\right]. \tag{36}$$

Note that in practice the emission intensities and top boundary values are constant over discrete time intervals (e.g. hourly) and the above forward Euler integration within such an interval is equivalent to Crank–Nicholson. The corresponding discrete adjoint model is also of the form (30).

From (30) and (36) one can easily obtain the cost functional derivatives with respect to other parameters. For example the adjoint sensitivities with respect to emission rates can be calculated by the transposed chain rule relation

$$\mu^n = \frac{\partial \mathscr{I}}{\partial Q(t^n)} = \left(\frac{\partial c^{n+1}}{\partial Q(t^n)}\right)^{\mathrm{T}} \cdot \frac{\partial \mathscr{I}}{\partial c^{n+1}} = \left(\frac{\partial c^{n+1}}{\partial Q(t^n)}\right)^{\mathrm{T}} \cdot \lambda^{n+1} = \frac{1}{\Delta z_1} e_1^{\mathrm{T}} \left(I - \frac{\Delta t}{2} A^{\mathrm{T}}(t^{n+1})\right)^{-1} \lambda^{n+1}. \tag{37}$$

The emission sensitivity μ^n is obtained at virtually no additional cost, since the vector $[I - (\Delta t/2)A^{\mathrm{T}}]^{-1}\lambda$ is already computed during the update of λ in (30).

4.3. Chemistry

Atmospheric chemical kinetics result in stiff ODE equations that require special numerical integration methods which are stable, preserve linear invariants (a.k.a. mass) and are computationally efficient. In [41], we have shown that Rosenbrock methods are well suited for solving atmospheric chemistry problems. The forward discrete chemical model in STEM is given by a Rosenbrock discretization of the chemical equations

$$Y_i = y_n + \sum_{j=1}^{i-1} a_{i,j} k_j,$$

$$\left(\frac{1}{h\gamma} - J(y_n)\right) k_i = f(Y_i) + \sum_{j=1}^{i-1} \frac{c_{i,j}}{h} k_j, \quad i = 1, \ldots, s, \tag{38}$$

$$y_{n+1} = y_n + \sum_{j=1}^{s} m_j k_j.$$

In [8,42], we show that the corresponding discrete adjoint reads

$$\left(\frac{1}{h\gamma} - J^{\mathrm{T}}(y_n)\right) u_i = m_i \lambda_{n+1} + \sum_{j=i+1}^{s} \left(a_{j,i} v_j + \frac{c_{j,i}}{h} u_j\right),$$

$$v_i = J^{\mathrm{T}}(Y_i) u_i, \quad i = s, s-1, \ldots, 1, \tag{39}$$

$$\lambda_n = \lambda_{n+1} + \sum_{i=1}^{s} \left(H(y_n) \times k_i\right)^{\mathrm{T}} \cdot u_i + \sum_{i=1}^{s} v_i.$$

Here J denotes the Jacobian and H (a 3-tensor) is the Hessian of the derivative function f. Y_i are the stage solution vectors computed by the forward method (38). The formulation can be easily extended to nonautonomous systems.

For completeness we give the continuous chemical adjoint model, obtained by solving the adjoint chemical equation with the Rosenbrock method (38)

$$\Lambda_i = \lambda_{n+1} + \sum_{j=1}^{i-1} a_{i,j} k_j, \quad Y_i = y(t_{n+1} - \alpha_i h)$$

$$\left(\frac{1}{h\gamma} - J^{\mathrm{T}}(y_{n+1})\right) k_i = J^{\mathrm{T}}(Y_i) \cdot \Lambda_i + \sum_{j=1}^{i-1} \frac{c_{i,j}}{h} k_j, \quad i = 1, \ldots, s, \tag{40}$$

$$\lambda_n = \lambda_{n+1} + \sum_{j=1}^{s} m_j k_j.$$

The numerical experiments reported here use the two stage, second order Rosenbrock method Ros-2 [49] which is defined by the coefficients $\gamma = 1 + \sqrt{2}/2$, $m_1 = 3/2$, $m_2 = 1/2$, $a_{2,1} = 1$, and $c_{2,1} = -2$.

Other popular numerical integration methods for stiff systems are Runge–Kutta and backward differentiation formulas (BDF). It can be shown [43] that the discrete adjoints of BDF schemes are in general (for variable step sizes) inconsistent with the continuous adjoint equation. Runge–Kutta and Rosenbrock methods on the other hand are well suited for adjoint computations [22,43].

The implementation of numerical integrators for chemistry can be done automatically using the Kinetic PreProcessor KPP software tools [11]. A related approach was taken in the early application of the 4D-Var to chemical data assimilation by Fisher and Lary [21]. KPP was recently extended [9,42] to produce a rapid and efficient implementation of the code for sensitivity analysis of chemical kinetic systems. KPP builds Fortran77, Fortran90, C, or Matlab simulation code for chemical systems with chemical concentrations changing in time according to the law of mass action kinetics. KPP generates the following building blocks:

1. *Fun*: the time derivative of concentrations;
2. *Jac, Jac_SP*: Jacobian of Fun in full or in sparse format;
3. *KppDecomp*: sparse LU decomposition for the Jacobian;
4. *KppSolve, KppSolveTR*: solve sparse system with the Jacobian matrix and its transpose;
5. *Jac_SP_Vec, JacTR_SP_Vec*: sparse Jacobian (transposed or not) times vector;
6. The stoichiometric matrix STOICM;
7. *ReactantProd*: vector of reaction rates;
8. *JacReactantProd*: the Jacobian of the above;
9. *dFun_dRcoeff*: derivatives of Fun with respect to reaction coefficients (in sparse format);
10. *dJac_dRcoeff*: derivatives of Jac with respect to reaction coefficients times user vector;
11. *Hess*: the Hessian of Fun; this 3-tensor is represented in sparse format;
12. *Hess_Vec, HessTR_Vec*: Hessian (or its transpose) times user vectors; same as the derivative of Jacobian (transposed) vector product times vector.

In [9,42] we show how these KPP building blocks can be used to implement very efficiently code for direct and adjoint sensitivity analysis of chemical systems.

5. Implementation aspects of adjoint STEM-III

The forward and adjoint models are parallelized and were run on a cluster of Linux workstations. Parallelization is based on dimensional splitting as supported by our library PAQMSG [39]. The library supports data types for structured grids, and implements routines for data decomposition, allocation of local and global entities, data scattering, gathering, and shuffling. We use the horizontal–vertical data decomposition presented in Fig. 2. With data in the horizontal slice format each processor can compute the horizontal transport; then data is shuffled in vertical column format and each processor can compute radiation, vertical transport, chemistry and aerosol processes in one column. For the horizontal transport the number of processor employed is at most the number of layers. Typically, about 90% of the computational effort is spent in radiation and chemistry computations, which use data in the column partitioned format. There are many columns which are mapped onto the available processors such that each processor receives about an equal amount of work. PAQMSG implements a static mapping scheme of columns (tasks) to processors that ensures a very good load balancing. On a cluster of workstations all input and output is handled by the master process (see Fig. 3); and all computations are done by the worker nodes.

For the adjoint we use a two-level checkpointing scheme. The level-2 checkpoints store the concentration fields on the disk at every operator split step (i.e. at every 15 min for the current application). Note that the linear transport scheme does not require any additional checkpointing storage. The amount of level-2 checkpoint data increases fivefold if a nonlinear transport scheme (e.g. using flux limiting) is used. The
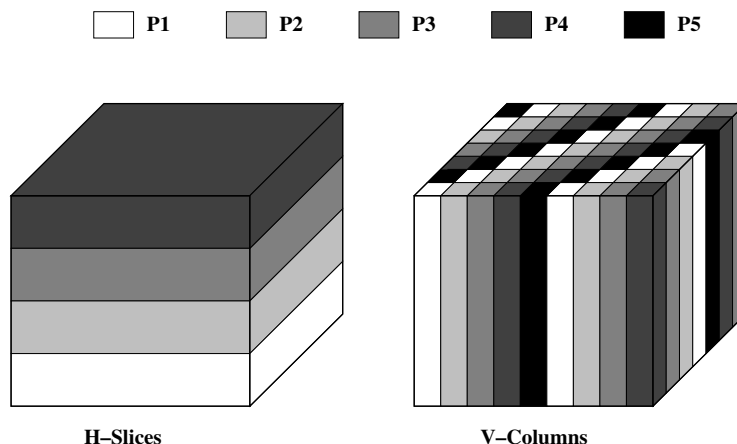
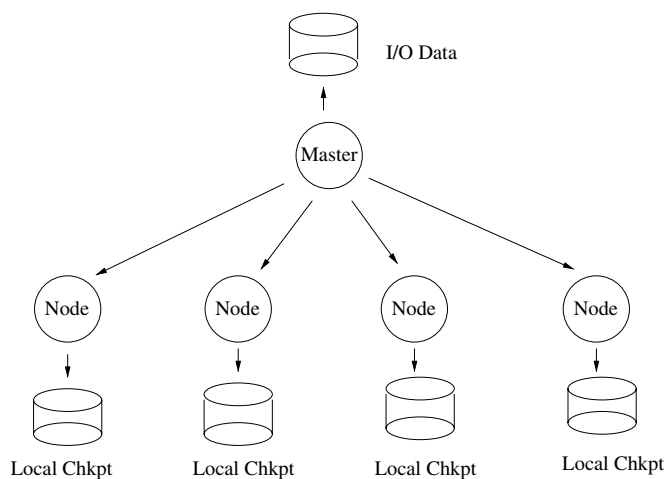Fig. 2. The horizontal–vertical data decomposition scheme supported by PAQMSG.

Fig. 3. The parallel adjoint STEM implements a distributed checkpointing scheme.

level-1 checkpoints store the concentrations for each process inside the 15 min intervals; level-1 checkpoints use memory buffers. For example one forward integration of each chemical box model for 15 min split time interval requires a number of smaller time steps; these intermediate concentrations are stored in a temporary matrix and used during the backward integration of the adjoint model. Operator splitting and the relative short split time intervals make it feasible to store the level-1 checkpoints in memory.

The gas phase chemical mechanism is SAPRC-99 [7] which considers the gas-phase atmospheric reactions of volatile organic (VOCs) and nitrogen oxides (NO_x) in urban and regional settings. The sparsity structure of the Jacobian is shown in Fig. 1. The forward time integration is done with the Rosenbrock numerical integrator Ros-2 [49]; the continuous adjoint model uses Ros-2 on the same sequence of steps as the forward chemical integration. Both the forward and the adjoint models are implemented using KPP.

For our East Asia application discussed in the following section the total level-2 checkpoint information stored is ~162 MBytes of data for each hour of simulation; or ~4 GBytes per 24 h of simulation. The level-2 checkpoints of the parallel model are distributed as shown in Fig. 3, where each node stores local

information on the local disk. This takes full advantage of the total storage capabilities of the system. It also decreases the communication overhead when the parallel computation runs on a cluster of workstations since the gigabytes of data are not transmitted over the (relatively slow) connection. The distributed checkpointing strategy is therefore essential for both efficiency and overall storage capacity. Note that for the static domain decomposition implemented in PAQMSG the local entities (i.e. horizontal slices or sets of columns of the concentration field) have the same size throughout the computation, which makes the implementation of the distributed checkpointing scheme very efficient. For a dynamic domain decomposition strategy, on the other hand, the size of local entities change during the computation and the implementation of distributed checkpointing becomes complicated.

The parallel performance of adjoint STEM-III is presented in Fig. 4. The East Asia test case is run on a Beowulf cluster with 20 nodes (Pentium 4, 2 GHz, 1 GB RAM) and Gigabit ethernet connection; the one hour forward and backward simulation corresponds to 0–1 GMT on March 1st, 2001. On 16 workers the absolute cpu time for a forward run is about 2 min per hour of simulation; and the cpu time for a forward–backward run is about 5 min per hour of simulation. The speedup curve (Fig. 4) is close to optimal; for 19 workers the speedup is 16, which translates into an efficiency of 85%.

6. Numerical results

The adjoint of the STEM chemical transport model can be used in sensitivity analysis studies and also for chemical data assimilation. We now present these two important applications of the computational tools developed. The analyzed problems are in support of the NASA TRAnsport and Chemical Evolution over the Pacific (Trace-P) field experiment conducted in East Asia. The simulated region covers 7200×4800 km in East Asia, and the simulated interval is one month starting at 0 GMT on March 1st, 2001. The meteorological fields are given by a dynamic meteorological model (RAMS) [40], and the initial fields and boundary conditions correspond to Trace-P data campaign. The grid has $90 \times 60 \times 18$ points with a horizontal resolution of 80 km $\times$ 80 km.

Details of the forward model simulation conditions and comparison with observations are presented in Carmichael et al. [6]. The time series of calculated O_3, NO_2, HCHO, and CO concentration are presented in
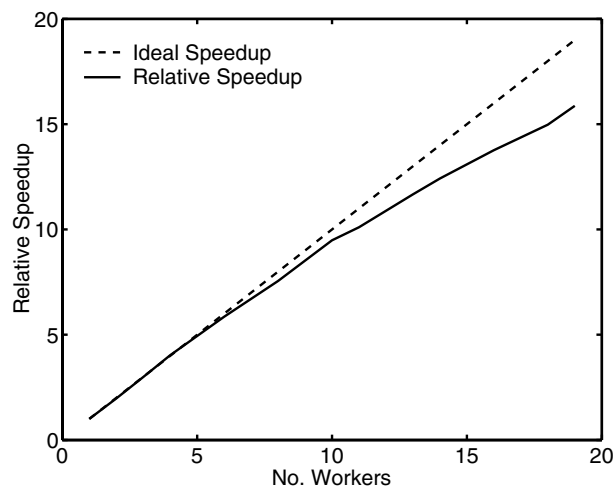

Fig. 4. Speedups (relative to a single worker process) for one hour of forward–backward integration with parallel adjoint STEM.

Fig. 5. Cheju island (longitude $\sim 127°$ E, latitude $\sim 34°$ N) is a remote location, but under the influence of emissions from China, Korea and Japan, depending on the outflow conditions. As shown in Fig. 5, CO and O_3 can reach values of ~ 450 and ~ 75 ppb, respectively. The time series show diurnal and synoptic scale variability that reflects the complex nature of the Asian outflow.

6.1. Adjoint sensitivity analysis

For the sensitivity analysis 10 simulation cases were carried out to cover the whole month of the Trace-P campaign period. They are listed in Table 1. The simulation interval for each case is three days. The first case starts at 0:00 GMT on March 1st, 2001, the second starts at 0:00:00 GMT on March 4th, 2001, and so forth. The response functional $g = g(c(t^F))$ is the ground level ozone concentration at Cheju Island, at the final time step of each case.

As shown in Section 3, sensitivities of the response functional $g = g(c(t^F))$ with respect to the state variables (at each time instant) are the adjoint variables $\lambda(t)$, which can be obtained by integrating the adjoint model backwards in time. The distributions of the adjoint variables in the three-dimensional computation domain, which are available at any instant, provide the essential information for the sensitivity analysis. For instance, isosurfaces of adjoint variables delineate "influence regions", i.e. areas where perturbations in some concentrations will produce significant changes in the response functional (e.g. ozone at Cheju Island at the final time).

Fig. 6 displays the influence areas of ozone at 24 h before the final time in case 2 (March 4–6) and case 9 (March 25–27), respectively. The influence region for case 9 is toward the South and close to the Cheju Island, while that for case 2 is toward the Northwest. This difference reflects different meteorological conditions, as indicated by the wind fields shown in Fig. 6.
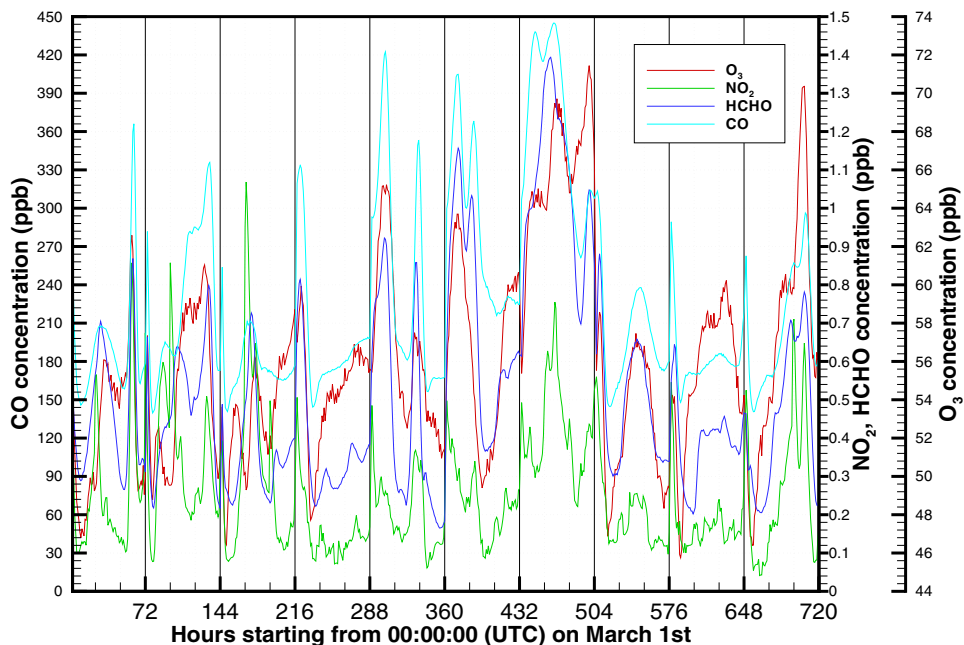

Fig. 5. Time series of concentrations at Cheju.

Table 1
Descriptions of simulation tests in the sensitivity analysis

Case	Simulation time period	Target function
1	March 1–3, 2001	Cheju O_3 at 0 GMT on March 04, 2001
2	March 4–6, 2001	Cheju O_3 at 0 GMT on March 07, 2001
3	March 7–9, 2001	Cheju O_3 at 0 GMT on March 10, 2001
4	March 10–12, 2001	Cheju O_3 at 0 GMT on March 13, 2001
5	March 13–15, 2001	Cheju O_3 at 0 GMT on March 16, 2001
6	March 16–18, 2001	Cheju O_3 at 0 GMT on March 19, 2001
7	March 19–21, 2001	Cheju O_3 at 0 GMT on March 22, 2001
8	March 22–24, 2001	Cheju O_3 at 0 GMT on March 25, 2001
9	March 25–27, 2001	Cheju O_3 at 0 GMT on March 28, 2001
10	March 28–30, 2001	Cheju O_3 at 0 GMT on March 30, 2001

Three-dimensional back trajectories calculated every 3 h during the periods of March 4–6 and March 25–27 for Cheju are shown in Fig. 7. The back trajectories provide important insight into the adjoint variable distributions. As shown in Fig. 6, for the March 4–6 case the flows are from the northwest and strong, such that air masses 24 h before arriving at Cheju were over the Beijing area at altitude generally below 2 km. In contrast, during March 22–24 Cheju was under the influence of a high pressure system, and 24 h before arriving at Cheju the flows were weak and from the south/south-west at altitude below ∼1 km. These features are seen in the influence areas for ozone both in terms of location of the upwind areas, and the proximity to Cheju (e.g., the influence area are much closer to Cheju for case 9 than for case 2).

The influence regions are difficult to predict based solely on meteorological fields, due to the influence of turbulent diffusion and complicated chemical reactions. Because of the turbulent nature of the atmospheric boundary layer, the influence region may quickly extend to a very large area, covering most of the computational domain, and even beyond that. The fact that influence regions cannot be simply predicted through the meteorological fields is indicated by the differences in the influence regions of various chemical components, even if they are all driven by the same wind field.
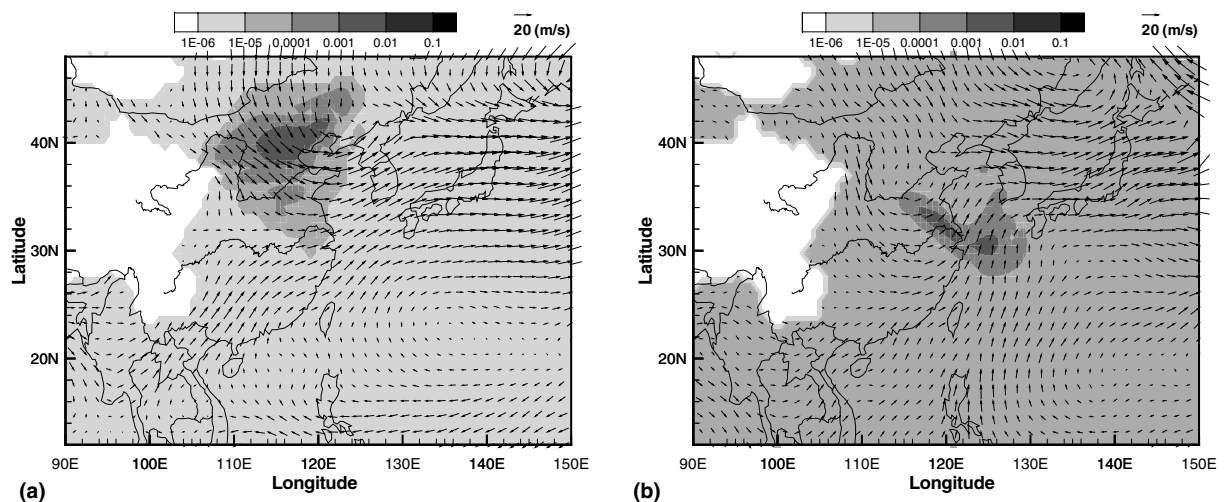

Fig. 6. Influence function λ_{O_3}, at 1.713 km above sea level, 24 h before the final time from (a) March 4–6, and (b) March 25–27. The target function is O_3 at Cheju.
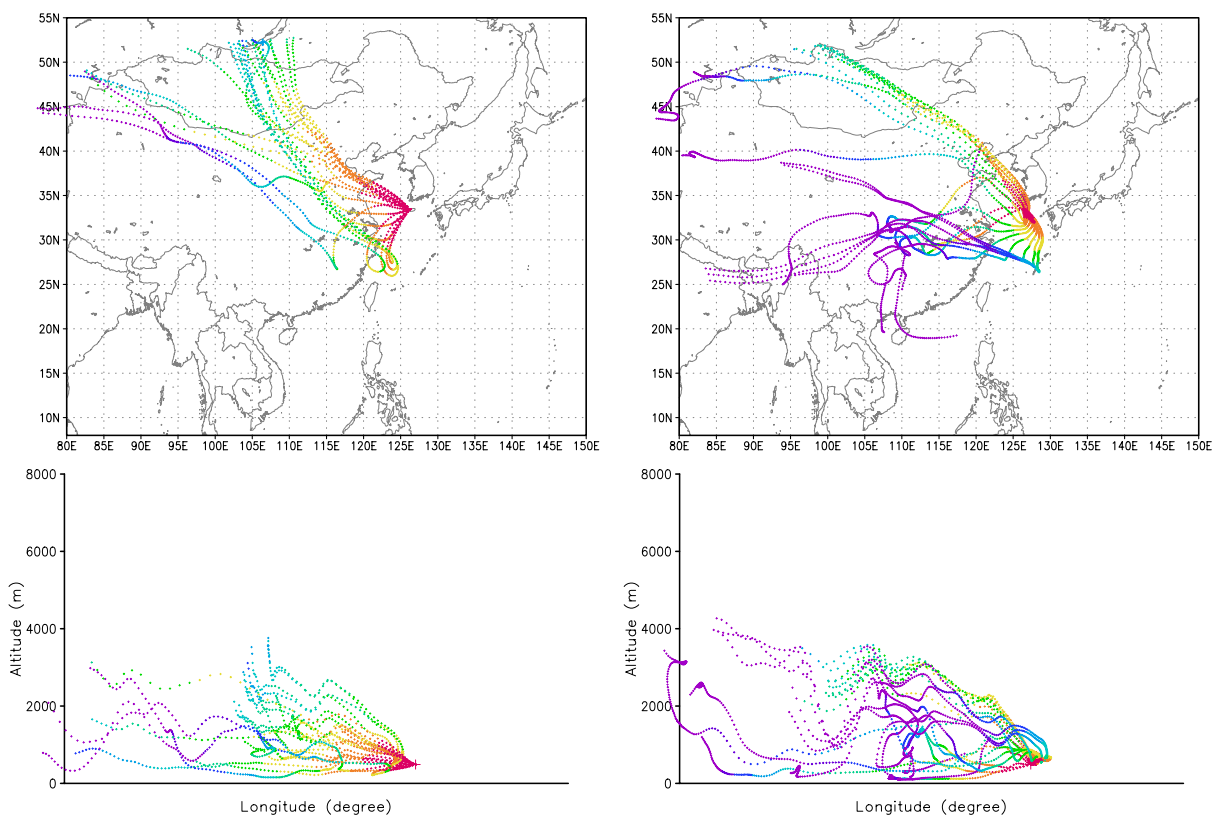
Fig. 7. Back trajectories starting at Cheju calculated every 3 h during the periods of March 4–6 (left) and March 22–26 (right).

In order to illustrate this fact, and to identify the region where changes of a certain chemical component will affect the target ozone observation most, adjoint variable magnitude are averaged for the period of three days for each case

$$\mathscr{C}_i(x) = \frac{1}{N} \sum_{i=0}^{N-1} |\lambda_i(x,t)|. \tag{41}$$

Higher values of $\mathscr{C}$ form "cones of influence", i.e. regions where concentration changes affect the target function most. Figs. 8 and 9 display these "cones of influence" for cases 2 and 9, respectively.

The "cones of influence" for case 2 show that the influence of ozone on itself is confined to regions within a transport time of less than 1.5 days from Cheju, while the major influence areas for HCHO are over the primary source regions around Beijing and $\sim$2 days removed from Cheju. The influence of NO_2 on ozone is far removed from Cheju, with the region of maximum influence location near the domain boundary and $\gtrsim 3$ days upwind of Cheju, at altitudes between 2 and 4 km. The trajectories shown in Fig. 7 help explain the vertical distribution of the cones of influence. However the fact that the influence of NO_2 is located farthest away reflects the fact that ozone is produced in the atmosphere via photochemical reactions involving NO_2. In the region of maximum O_3 sensitivity to NO_2, ozone production is NO_2-limited and increases in NO_2 lead to increases in O_3 levels. This process is fast, and the NO_2 lifetime and transport distance are short, so that the ozone is enhanced locally and then transported to Cheju. In addition, ozone production

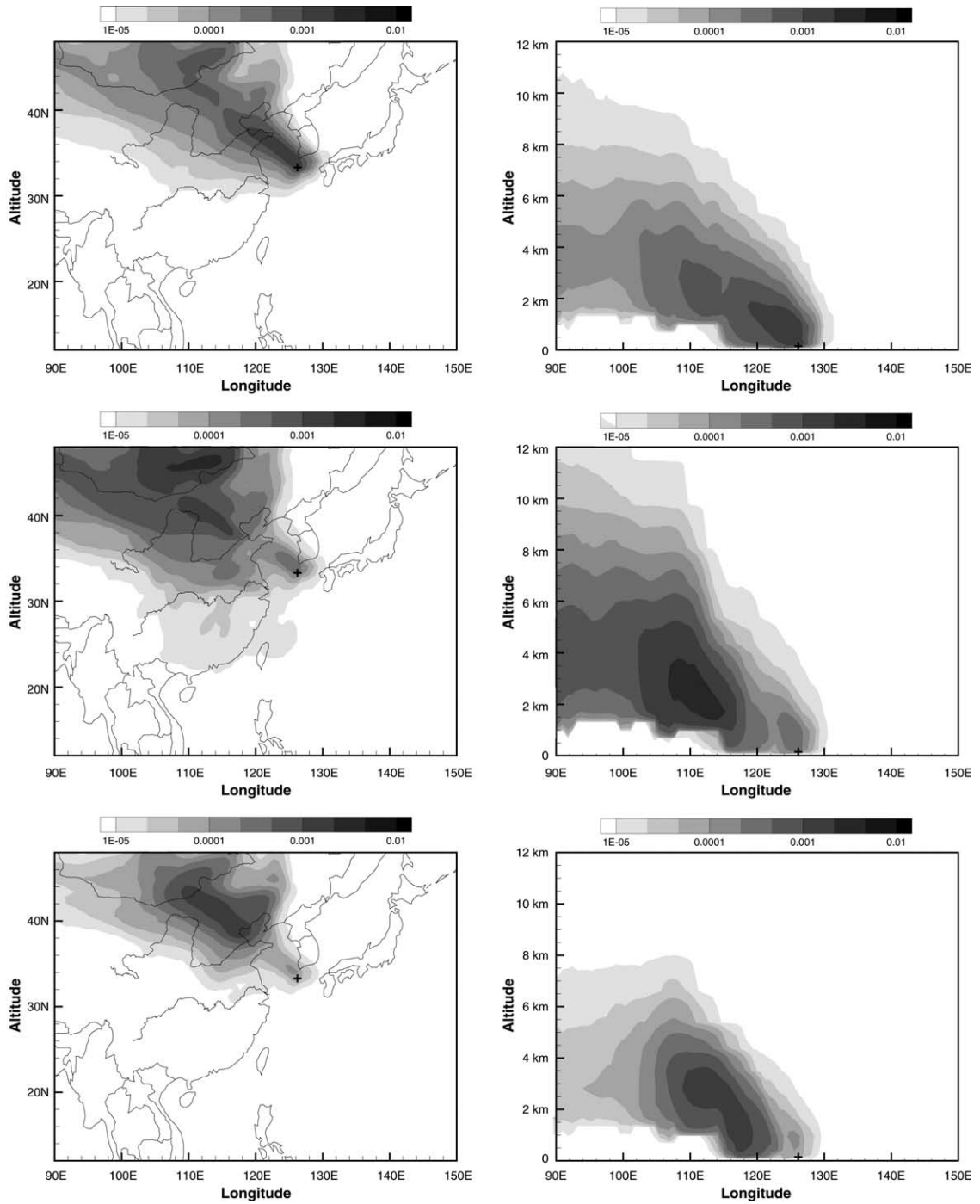Fig. 8. Cones of influence for March 4–6. Cheju Island marked with "+". From top to bottom: O_3, NO_2, and HCHO. Contours of averaged $\mathscr{C}$ over levels below 5 km are shown on the left. On the right, maximum $\mathscr{C}$ in north-south direction are used to illustrate the cones of influence.
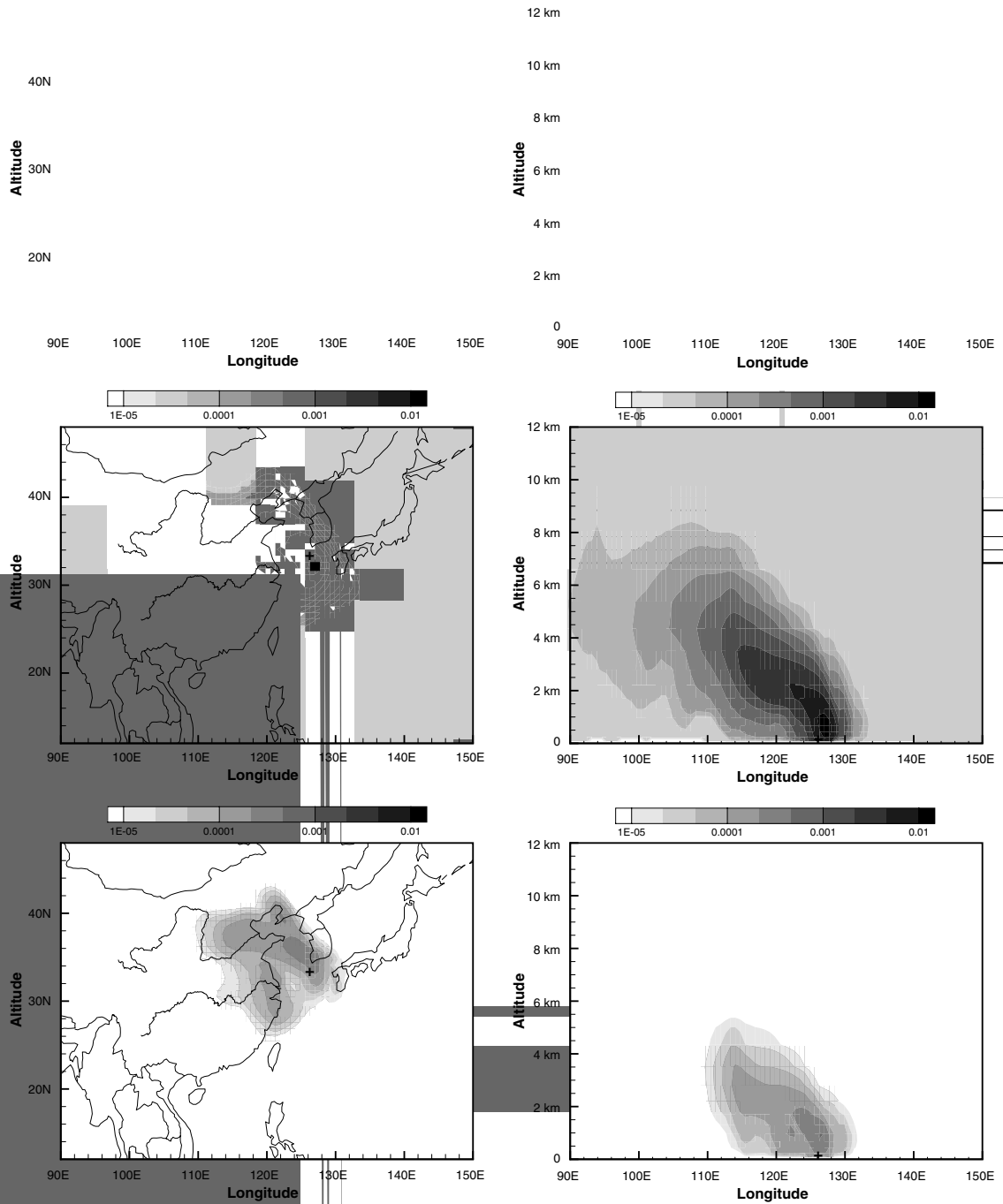
Fig. 9. Cones of influence for March 25–27. Cheju Island marked with "+". From top to bottom: O_3, NO_2, and HCHO. On the right, maximum $\mathscr{C}$ in north-south direction are used to illustrate the cones of influence.

along the path from Beijing to Cheju is NMHC-limited [6] and the increases in NO_2 result in a decrease in ozone.

The situation for case 9 is very different, with the "cones of influence" located around Cheju, and of limited vertical extent. These features reflect the influence of the high pressure system.

Further insights into the information contained in the adjoint sensitivities are obtained from Figs. 10–13. They illustrate, for each of the 10 cases analyzed, the ozone sensitivities at Cheju at the end of each simulation period with respect to perturbations in surface layer O_3, NO_2, HCHO, and CO at any time within the simulation window. In the figures, the solid lines represent the time series of the adjoint sensitivities for perturbation to species concentration at Cheju, while the dots represent sensitivities due to perturbation of surface concentration at every grid within the domain. The locations of the maximum value for each of the 10 cases for each species are shown in Fig. 14.

The time series of adjoint variables provides insight into the relative impact of transport and chemistry. For example, for a pure tracer under the influence of advection only (no diffusion, real or numerical), the adjoint time series with respect to itself would be a delta function with value of unity at the end of each 3 day period and zero for all times prior. Under these conditions, the sensitivity of the tracer with respect to all other species would be zero at all times.

The calculated ozone sensitivity with respect to itself shows the strong influence of transport for most of the periods studied (e.g., cases 1–7, and 10). Here the ozone values are largest for the times closer to the last time step. (Note that in order to produce the time series shown, the value of unity at the end of each period is not plotted, but instead the value for the first time step of the next case is shown.)

For these cases the ozone time series are qualitatively similar, with adjoint sensitivity increasing after ~48 h, then becoming negative at ~50 h, and then increasing, reaching a maximum positive value during
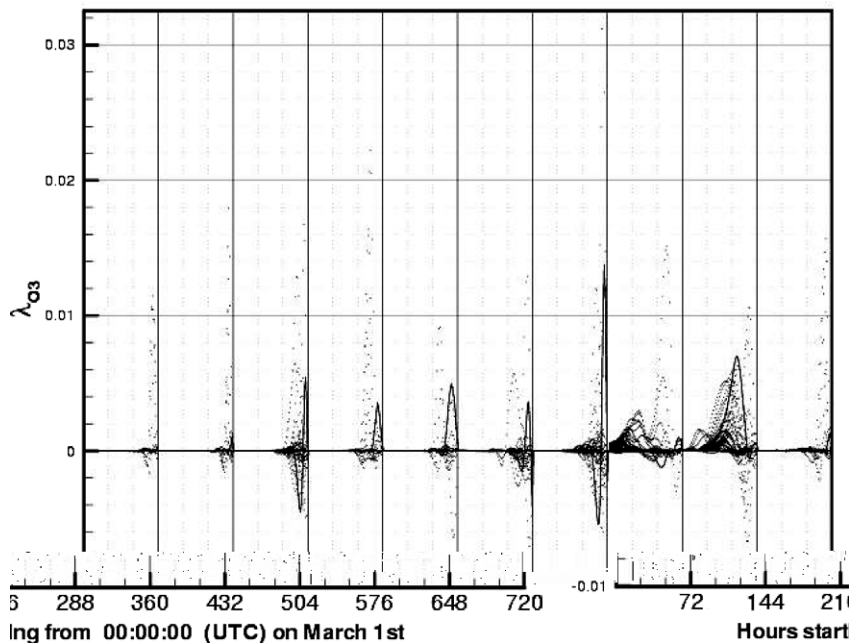

Fig. 10. Time series of λ_{O_3}, the adjoint sensitivities of surface ozone at Cheju with respect to perturbation of surface O_3. The solid lines represents the sensitivity to O_3 concentration at Cheju, while the dots represent sensitivities to O_3 perturbations at every grid within the domain.
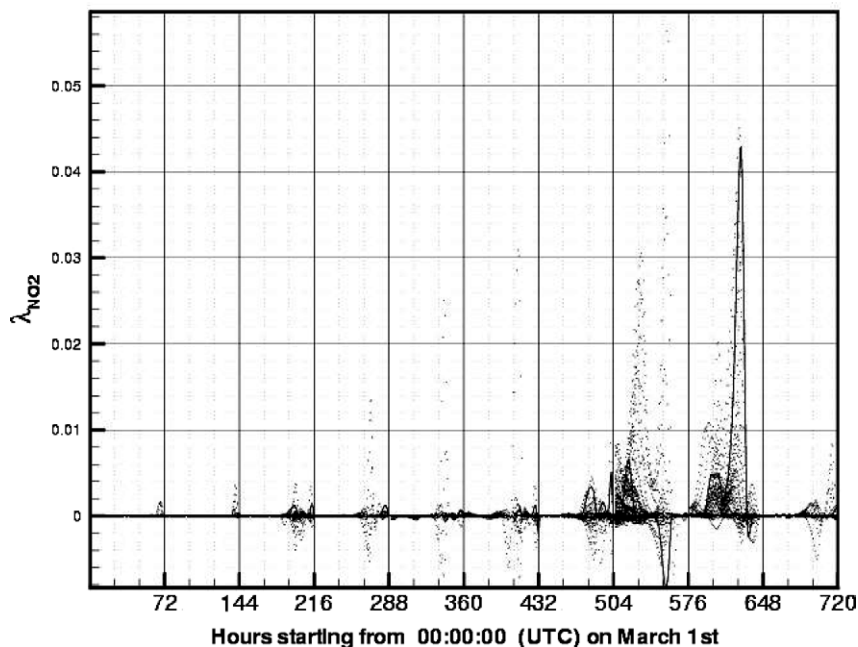
Fig. 11. Time series of λ_{NO_2}, the adjoint sensitivities of surface ozone at Cheju with respect to perturbation of surface NO_2. The solid lines represents the sensitivity to NO_2 concentration at Cheju, while the dots represent sensitivities to NO_2 perturbations at every grid within the domain.

the period 60–70 h. A positive λ_{O_3} implies a increase of surface ozone at Cheju at some time (e.g., hour 60) will incur an increase in ozone at hour 72. This can happen only through diffusion or if the trajectories recycle around Cheju. A negative sensitivity for O_3 with respect to O_3 implies that an increase in ozone at some previous time leads to a decrease in ozone at Cheju at the end of the 3-day simulation. This can only occur through chemical interactions under conditions when increasing ozone decreases future ozone production via reduction in NO_2 andor peroxyl radicals. This phenomena occurs for most periods around sunset of the 3rd day of the simulation. The behavior during the stagnant high pressure cases (cases 8 and 9, hours 504–648) is different, and show a broad influence over the entire 3 day period. This reflects the recycling of trajectories (as shown in Fig. 7) along with diffusion.

The surface behavior of the surrounding grid cells are qualitatively similar to that for for Cheju (dots vs line) in terms of time period of influence, and show positive and negative interactions, but with maximum values occurring at locations other than Cheju (This is discussed in more detail later).

The adjoint sensitivities of surface ozone at Cheju with respect to perturbation of surface NO_2 are shown in Fig. 11. Increasing NO_2 can increase ozone production under NO_x-limited chemical conditions, and can decrease ozone under VOC-limited condition (by decreasing peroxyl radical concentrations). Both behaviors are shown. Under strong transport conditions the sensitivities with respect to NO_2 are generally smaller than those for ozone. However, under the high pressure condition the sensitivities with respect to NO_2 are larger than those for ozone. For case 8, the largest positive sensitivities occurred 2.5 days in advance.

The sensitivities of ozone with respect to HCHO perturbation are much smaller than those for ozone and NO_2, but show similar pattern to those for ozone. HCHO is both a primary and secondary species. The sensitivities of ozone with respect to CO are extremely small, representing the weak interaction between CO and ozone on these time scales. CO influences ozone via altering the OH concentration ($\uparrow$CO leads to $\downarrow$OH).
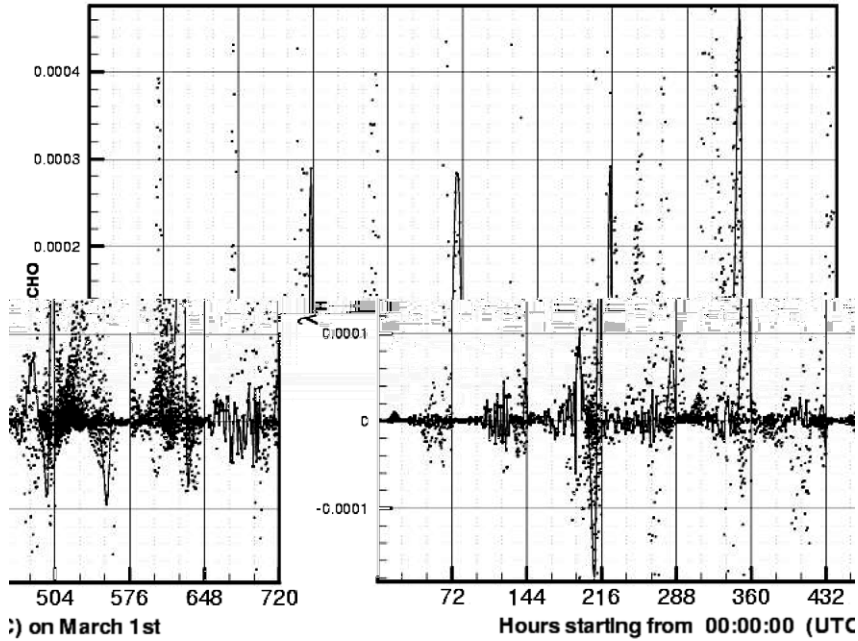
Fig. 12. Time series of λ_{HCHO}, the adjoint sensitivities of surface ozone at Cheju with respect to perturbation of surface HCHO. The solid lines represents the sensitivity to HCHO concentration at Cheju, while the dots represent sensitivities to HCHO perturbations at every grid within the domain.
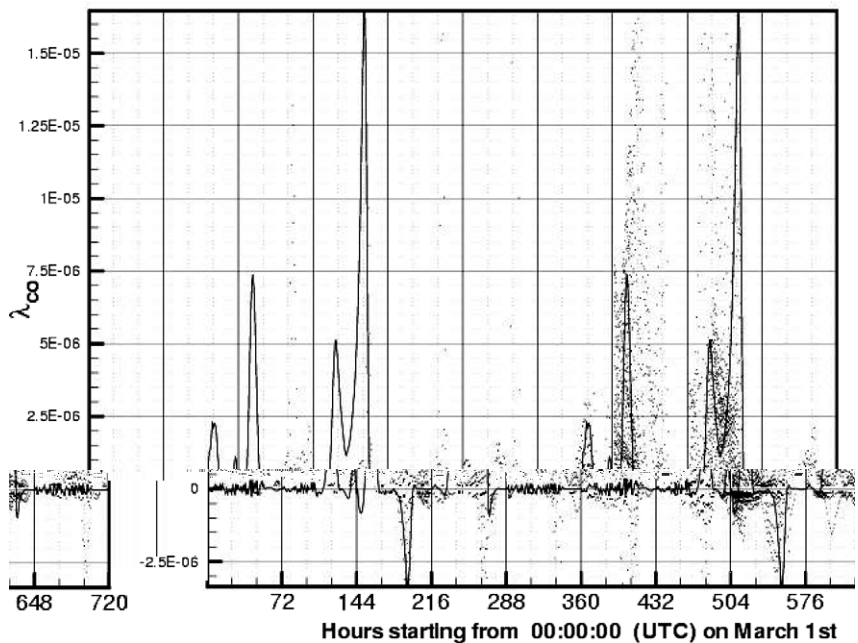

Fig. 13. Time series of λ_{CO}, the adjoint sensitivities of surface ozone at Cheju with respect to perturbation of surface CO. The solid lines represents the sensitivity to CO concentration at Cheju, while the dots represent sensitivities to CO perturbations at every grid within the domain.
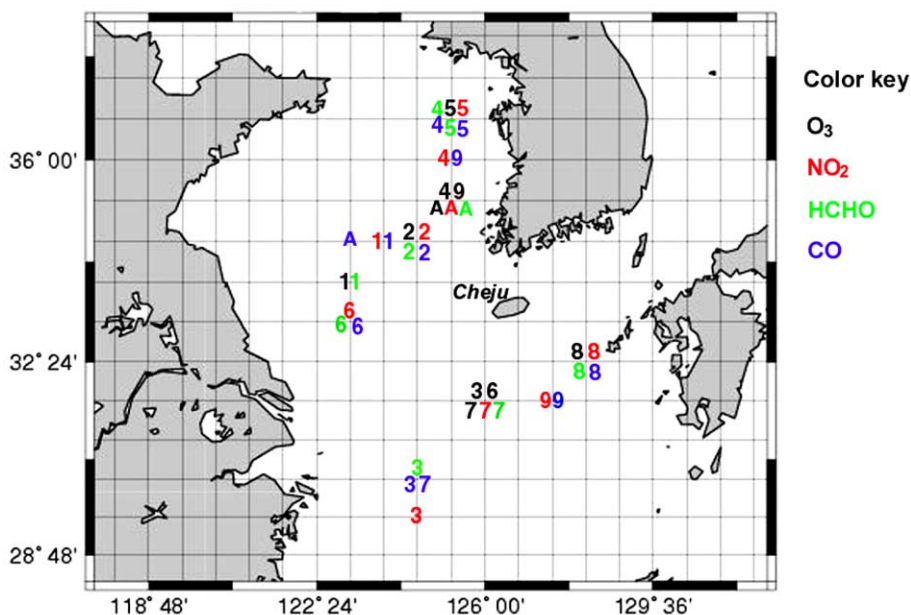
Fig. 14. Locations of the maximum sensitivity with respect to different species (color keyed) for all 10 cases (indicated by the case number, with "A" representing case 10).

The locations of the maximum sensitivities with respect to O_3, NO_2, HCHO, and CO for the individual 10 cases are shown in Fig. 14. Here the locations of the maximum (positive) sensitivity value anytime during the 3-day period for each case are plotted. The locations of the maximum values for cases 1, 2, 4, 5, and 10 fall in the NW sector. Under the strong outflow conditions represented by these cases (cf., the trajectories, for case 2 shown in Fig. 7), the location for all the maximum values occur at the same location, indicating that locations are determined by the transport. The locations of the maximum values for cases 7 and 8 fall in S, SE of Cheju (see Fig. 7 for trajectories). When the trajectories during a period vary greatly the locations of the maximum values differ by species (e.g., case 9).

The dependence of the "regions/cones of influence" on meteorological conditions imply that the computed cones are at most as accurate as are the meteorological fields supplied to the simulation. In addition, their accuracy is impacted by the numerical errors in the solutions of both the forward and the adjoint models.

6.2. Data assimilation

The preliminary data assimilation tests were conducted in the twin experiments framework. The descriptions are as follows:

- *Reference run*: The reference model run starts at $t^0 = 0:00$ GMT on March 1st, with the reference initial concentrations of all chemical species.
- *Observations and assimilation window*: We consider a 6 h assimilation window. The observations are concentrations of selected species Y_0^{obs} (here O_3 and NO_2) as computed by the reference run. Observations are provided on all grid points at the end of the assimilation window $t^0 + 6h$.
- *Parameters*: The control parameters are the initial concentrations of selected species $Y_c(t^0)$ (here O_3 or NO_2).

- *Initial guess*: The initial values of the control species are increased by 20%. This provides the "background" values Y_b, which are used as initial conditions for the initial guess run.
- *Cost functional*: Measures the distance between the model predictions Y_0 and the values Y_0^{obs} of the selected observed species, as well as the deviation of control variables from the background state.

$$\mathcal{J}\left(Y_c(t^0)\right) = \frac{1}{2b} \sum_{\text{gridpoints}} \left[Y_c(t^0) - Y_b\right]^2 + \frac{1}{2r} \sum_{\text{gridpoints}} \left[Y_0(t^F) - Y_0^{obs}(t^F)\right]^2. \tag{42}$$

The background and measurement covariance matrices are diagonal,

$$B = \text{diag}\{b\}, \qquad R = \text{diag}\{r\}, \tag{43}$$

with $b = 1000$ and $r = 1$, which means we trust the measurements considerably more than the background state.

- *Optimization algorithm*: Quasi-Newton limited memory L-BFGS [2]. The optimization proceeds until the cost functional is reduced to 0.001 of its initial value, or the number of forward–backward model integrations exceeds 15.

To simplify the data assimilation tests, we only choose the initial O_3 (or NO_2) concentrations as control variables while the initial concentrations of other species are kept at their reference values. This gives somewhat idealized test conditions. The control variables (initial concentrations of O_3, NO_2) are perturbed by 20% from their reference values. The observed variables are O_3 and/or NO_2. We found that assimilating O_3 observations alone brings little change to initial concentrations of other species, while assimilating some other species does bring up adjustments of several initial concentrations.

The performance of the data assimilation procedure is measured by the RMS difference between the reference values of the control variables and their values recovered by data assimilation. The RMS errors shown in Fig. 15 are defined as
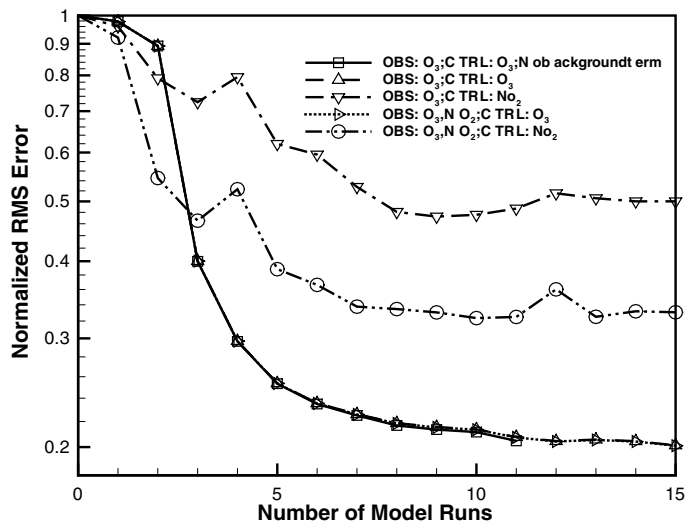

Fig. 15. Data assimilation results: RMS errors of the control variables at the initial time (normalized by their pre-assimilation values) decrease during the optimization procedure. Several tests are shown using different control (CTRL) and observed (OBS) variables.

$$\text{RMS error} = \left(\max_{\text{gridpoints}} Y_c^{\text{reference}}\right)^{-1} \sqrt{\sum_{\text{gridpoints}} \left(Y_c(t^0) - Y_c^{\text{reference}}\right)^2 \left(\sum_{\text{gridpoints}} 1\right)^{-1}}. \tag{44}$$

The decrease in the RMS error of control variable values versus the number of model runs during the optimization procedure is shown in Fig. 15.

For O_3 control variables the optimization procedure produces a rapid decrease in the RMS error. Most of the information comes from O_3 observations; additional NO_2 observations do not seem to bring noticeable benefits. This may be due to the lack of scaling in our formulation of the cost functional. These results imply that ozone initial conditions is recoverable through data assimilation. For comparison we include the optimization of the cost functional without the background term (corresponding to an infinite background covariance). As expected the cost function decreases further.

For NO_2 control variables the decrease in the cost function, and in the RMS error, is not as pronounced as that for O_3. Again most of the information comes form O_3 measurements, with additional NO_2 measurements contributing very little to the optimization process. After about 10 model runs the RMS errors tend to stagnate, even if the cost functional continues to decrease. Perturbing the initial NO_2 concentration by 20% results in only a small change in the final (observed) O_3 concentration. This may be explained by the fact that NO_2 levels are driven mostly by emissions, and less by the initial conditions, which affects the observability of the initial NO_2 field through ozone measurements. The results indicate that further algorithmic developments are needed for assimilating NO_2. In particular a better scaling of the cost function, through a rigorous definition of the covariance matrices, is necessary.

It is interesting to note that the assimilated results in the central region are significantly better than the other regions. The decrease of the RMS error calculated in the central 50×20 grid points is plotted in Fig. 16 along with that of the RMS error calculated in the whole domain. This is probably because the concentrations in the central small region predicted at the final time step are more dependent on the initial condition than the boundary conditions, such as the effect of the ground emissions of some species. When pinpointing the assimilation result to specific locations, we also found very different features. For instance, Fig. 17 shows the progress of the recoveries of the O_3 concentrations at Cheju and Shanghai. When the
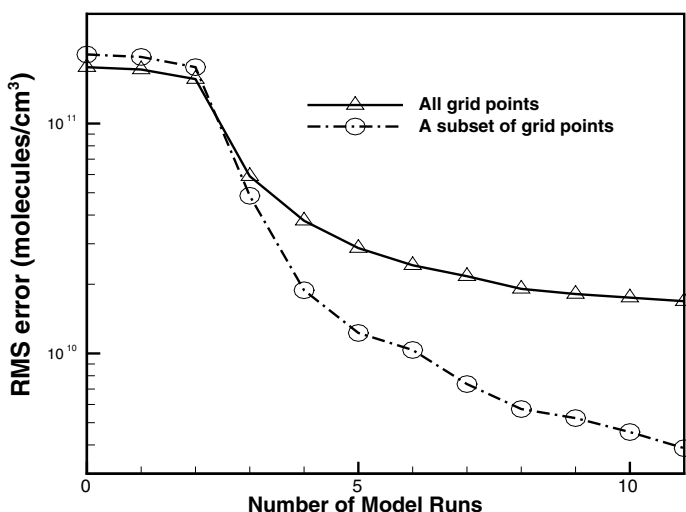

Fig. 16. Comparison of decrease of RMS errors calculated with all grid points and inner 50×20 ones. The small set of grid points are chosen to be horizontally centered, vertically spanning from grid levels 6–13. OBS: O_3, CTRL: O_3.
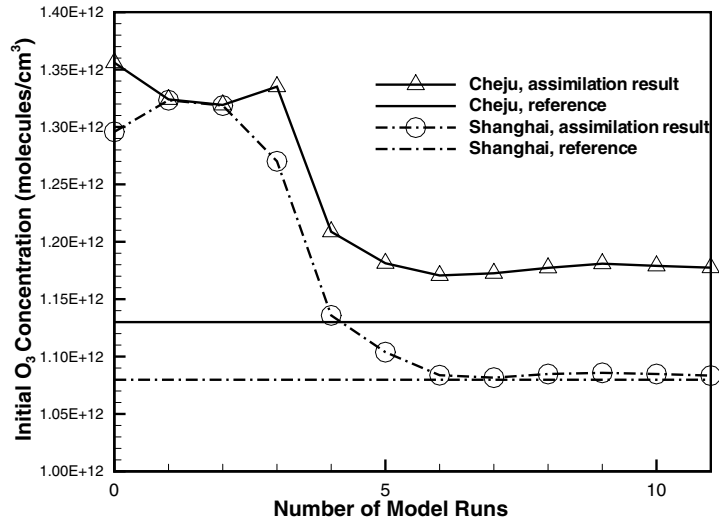
Fig. 17. Comparison of assimilation result at Cheju and Shanghai. Recovered initial O_3 concentrations are plotted at each iteration, with the reference values also shown. OBS: O_3, CTRL: O_3.

assimilation test stops after the cost functional has been reduced by more than three orders of magnitude, the O_3 prediction at Shanghai matches the exact value very well, which is anticipated. Unfortunately, the simulated O_3 concentration at Cheju is not as good, with the relative error only reduced from initial 20% to 6% at the end. This might suggest that the successful assimilation would require dense observation sites

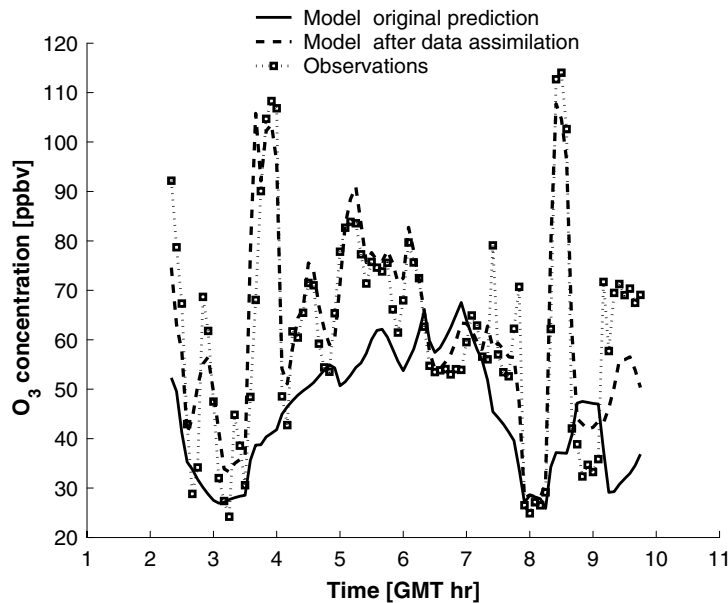

Fig. 18. Data assimilation results for O_3, P3-B observations on March 7, 2001. The initial ozone concentrations at all gridpoints are the control variables. The assimilation interval is 12 h. One notices the excellent agreement of the model predictions with the observations for the run after analysis.

close to the interest area rather than an uniformly distributed network, as our synthetic observation sites indicated. Work on this subject is obviously needed in the near future.

We conclude with results from the assimilation of a real data set. The O_3 observations collected during the Trace-P campaign by the P3-B flight on March 7, 2001, are shown in Fig. 18 (squares). This data set is assimilated in the window 0–12 GMT of March 7. The initial ozone concentrations at all gridpoints are the control variables. The initial model predictions (Fig. 18, solid line) do not reproduce well the observations. After analysis the model predictions (dashed line) are in excellent agreement with the observations.

7. Conclusions and future work

In this paper, we discuss the adjoint sensitivity analysis of three dimensional atmospheric transport and chemistry models. Adjoint modeling proves to be a powerful computational tool for sensitivity studies as well as for integrating observational data into the model in a four-dimensional variational (4D-Var) data assimilation procedure.

An overview of the mathematical theory of adjoint modeling applied to convection-diffusion-reaction models of atmospheric pollutants is given. The continuous and discrete adjoint model approaches are outlined, and formulations of the forcing terms for different cost functionals are discussed.

As an example of the discrete approach we discuss in detail the construction of the adjoint model of the comprehensive 3D chemical transport model STEM. Algorithmic details include the construction of adjoints for finite difference transport numerical schemes and for Rosenbrock integrators for stiff chemical kinetics. Implementation aspects including the parallelization, the efficient distributed checkpointing scheme, and the performance of the parallel adjoint code are also presented.

The use of adjoints for sensitivity analysis and for data assimilation problems is illustrated using numerical simulations of air pollution in East Asia. The analyzed problems are in support of the large Trace-P experiment conducted in East Asia in March 2001.

For sensitivity studies the target function is the ozone concentration at Cheju Island. Isosurfaces of adjoint variables delineate "influence regions", i.e. areas where perturbations in some concentrations will produce significant changes in this response functional. Results show that the influence regions are most affected by the meteorological fields, however they are difficult to predict from the meteorological information alone due to the influence of turbulent diffusion and complicated chemical reactions. The influence areas intersecting domain boundaries indicate that uncertainties in boundary values impact the accuracy of ozone predictions at Cheju Island. The cones of influence, defined by isosurfaces of the time integral of adjoint sensitivities, are useful to analyze the complex ozone production and transport processes.

The first set of data assimilation experiments are conducted in the twin experiment framework. We consider several scenarios, with the control variables being O_3 or NO_2, and the observed variables being O_3 and/or NO_2. The performance of the data assimilation procedure is measured by two indicators, the cost function value and the RMS error of control variables. The initial O_3 control variable can be recovered nicely from measurements through 4D-Var data assimilation. The recovery of the initial NO_2 concentrations is more difficult, presumably due to the fact that NO_2 levels are driven mostly by emissions.

Preliminary results from the assimilation of real data from the Trace-P campaign are presented. The excellent agreement of model predictions with observations after analysis constitutes another validation of the computational tools discussed in the paper.

Future work will focus on continuing the development of algorithmic and software infrastructure for adjoint modeling of comprehensive chemical transport models; and on using this computational infrastructure to run more complex tests and to assimilate real measurements data. The fundamental goal of this work is to enable the assimilation of chemical data available from ground, airplane, and satellite measurements into the models.

Acknowledgement

Appendix A. The tangent linear model and its adjoint

An infinitesimal perturbation δc^0 in the initial state will induce a variation $\delta \mathscr{J}$ in the response functional (4). To first order approximation,

$$\delta \mathscr{J} = \int_{t^0}^T dt \int_{\Omega} \delta c(t, \xi) \cdot \frac{\partial g}{\partial c}(c(t, \xi)) d\xi, \tag{A.1}$$

where the perturbations $\delta c(t,x)$ in the concentration fields are obtained by solving the tangent linear model

$$\frac{\partial \delta c_i}{\partial t} = -u \cdot \nabla \delta c_i + \frac{1}{\rho} \nabla \cdot (\rho K \nabla \delta c_i) + F_{i,*}(\rho c)\delta c, \quad t^0 \leqslant t \leqslant T, \tag{A.2a}$$

$$\delta c_i(t^0, x) = \delta c_i^0(x), \tag{A.2b}$$

$$\delta c_i(t, x) = \delta c_i^{IN}(t, x) = 0 \quad \text{for } x \in \Gamma^{IN}, \tag{A.2c}$$

$$K \frac{\partial \delta c_i}{\partial n} = 0 \quad \text{for } x \in \Gamma^{OUT}, \tag{A.2d}$$

$$K \frac{\partial \delta c_i}{\partial n} = V_i^{dep} \delta c_i \quad \text{for } x \in \Gamma^{GR}. \tag{A.2e}$$

In the above F is the Jacobian of the function f, and $F_{i,*}$ denotes its ith row. We refer to (A.2a)–(A.2e) as the *tangent linear model* associated with the forward model (1a)–(1e). In a compact notation

$$\frac{\partial \delta c}{\partial t} = \mathscr{L}(c(t))\delta c, \quad t^0 \leqslant t \leqslant T, \tag{A.3}$$

with the initial condition (A.2b). The domain $\mathscr{D}(\mathscr{L})$ of the linearized convection-diffusion-reaction operator $\mathscr{L}(c)$ is taken as the subspace $[C([t^0, T], C^2(\Omega))]^s \cap [C^1([t^0, T], L^2(\Omega))]^s$ of the Hilbert space $[L^2((t^0, T) \times \Omega)]^s$ constrained by the boundary conditions (A.2c)–(A.2e). In the direct sensitivity analysis approach one solves the model (1a)–(1e) together with the tangent linear model (A.2a)–(A.2e) forward in time (for each parameter an additional sensitivity equation must be solved). The equations (A.2a)–(A.2e) are of convection-diffusion-reaction type (with linearized chemistry) and in practice are solved by the same numerical method as the forward model (2) and (3); computational savings are possible by reusing the same matrix factorizations [51].

The adjoint method may be used to provide an explicit dependence of the response functional to variations in the parameters. The adjoint operator

$$\mathscr{L}^*(c)\lambda = \nabla \cdot (u\lambda) + \nabla \cdot \left(\rho K \nabla \frac{\lambda}{\rho} \right) + F^T(\rho c)\lambda$$

is determined from the Lagrange identity

$$\int_{t^0}^T dt \int_{\Omega} \mathscr{L}(c)\delta c \cdot \lambda \, dx = \int_{t^0}^T dt \int_{\Omega} \delta c \cdot \mathscr{L}^*(c)\lambda \, dx, \quad \forall \delta c \in \mathscr{D}(\mathscr{L}), \forall \lambda \in \mathscr{D}(\mathscr{L}^*). \tag{A.4}$$

The domain $\mathscr{D}(\mathscr{L}^*)$ of the adjoint operator is the subspace of $[C([t^0,T],C^2(\Omega))]^s \cap [C^1([t^0,T],L^2(\Omega))]^s$ constrained by the boundary conditions (5c)–(5e). Next, the inner product of (A.3) with $\lambda(t,x)$ is taken in $[L^2((t^0,T) \times \Omega)]^s$ to obtain

$$\int_{t^0}^{T} dt \int_{\Omega} \frac{\partial \delta c}{\partial t} \cdot \lambda dx = \int_{t^0}^{T} dt \int_{\Omega} \mathscr{L}(c(t)) \delta c \cdot \lambda \, dx. \tag{A.5}$$

After integrating by parts and using (A.4) it follows that

$$\int_{\Omega} \delta c(T) \cdot \lambda(T) dx - \int_{\Omega} \delta c(t^0) \cdot \lambda(t^0) dx = \int_{t^0}^{T} dt \int_{\Omega} \left(\frac{\partial \lambda}{\partial t} + \mathscr{L}^*(c)\lambda \right) \cdot \delta c.$$

If $\lambda(t,x) \in \mathscr{D}(\mathscr{L}^*)$ is defined as the solution of the adjoint problem

$$\frac{\partial \lambda}{\partial t} = -\mathscr{L}^*(c)\lambda - \frac{\partial g}{\partial c}(c(t,x)), \tag{A.6a}$$

$$\lambda(T) = 0, \tag{A.6b}$$

then

$$\delta \mathscr{I} = \int_{\Omega} \delta c^0 \cdot \lambda(t^0) dx,$$

such that $\lambda(t^0,x)$ represents the sensitivity to initial conditions.

References

[1] A.E. Bryson, Y.-C. Ho, Applied Optimal Control: Optimization, Estimation, and Control, Hemisphere Publishing Corporation, Washington, DC, 1975.
[2] R. Byrd, P. Lu, J. Nocedal, A limited memory algorithm for bound constrained optimization, SIAM J. Sci. Stat. Comput. 16 (5) (1995) 1190–1208.
[3] D.G. Cacuci, Sensitivity theory for nonlinear systems. I. Nonlinear functional analysis approach, J. Math. Phys. 22 (1981) 2794–2802.
[4] D.G. Cacuci, Sensitivity theory for nonlinear systems. II. Extensions to additional classes of responses, J. Math. Phys. 22 (1981) 2803–2812.
[5] G.R. Carmichael, A. Sandu, F.A. Potra, V. Damian-Iordache, Sensitivity analysis for atmospheric chemistry models via automatic differentiation, Atmos. Environ. 31 (3) (1997) 475–489.
[6] G.R. Carmichael, Y. Tang, G. Karata, I. Uno, D. Streets, N. Thongboonchoo, J.H. Woo, S. Gutikunda, A. White, T. Wang, D.R. Blake, E. Atlas, A. Fried, B. Potter, M.A. Avery, G.W. Sachse, S.T. Sandholm, Y. Kondo, R.W. Talbot, A. Bandy, D. Thornton, A.D. Clarke, Regional-Scale Chemical Transport Modeling in Support of the Analysis of Observations obtained During the Trace-P Experiment, J. Geophys. Res. 108 (D21) (2003) 8823.
[7] W.P.L. Carter, Implementation of the saprc-99 chemical mechanism into the models-3 framework. Technical report, United States Environmental Protection Agency, January 2000.
[8] D.N. Daescu, G.R. Carmichael, A. Sandu, Adjoint implementation of Rosenbrock methods applied to variational data assimilation problems, J. Computat. Phys. 165 (2000) 496–510.
[9] D.N. Daescu, A. Sandu, G.R. Carmichael, Direct and adjoint sensitivity analysis of chemical kinetic systems with KPP: II – numerical validation and applications, Atmos. Environ. 37 (2003) 5097–5114.
[10] D.N. Daescu, Theoretical and practical aspects of data assimilation for air pollution models, Ph.D. Dissertation in Applied and Computational Mathematics, the University of Iowa, 2001.
[11] V. Damian, A. Sandu, M. Damian, F. Potra, G.R. Carmichael, The kinetic preprocessor kpp – a software environment for solving chemical kinetics, Comp. Chem. Eng. 26 (2002) 1567–1579.
[12] A.M. Dunker, G. Yarwood, J.P. Ortmann, G.M. Wilson, Comparison of source appointment and source sensitivity of ozone in a three-dimensional air quality model, Environ. Sci. Technol. 36 (2002) 2953–2964.
[13] A.M. Dunker, G. Yarwood, J.P. Ortmann, G.M. Wilson, The decoupled direct method for sensitivity analysis in a three-dimensional air quality model – implementation, accuracy, and efficiency, Environ. Sci. Technol. 36 (2002) 2965–2976.

[14] H. Elbern, H. Schmidt, A 4D-Var chemistry data assimilation scheme for Eulerian chemistry transport modeling, J. Geophys. Res. 104 (5) (1999) 18–583.

[15] H. Elbern, H. Schmidt, Ozone episode analysis by 4D-Var chemistry data assimilation, J. Geophys. Res. 106 (D4) (2001) 3569–3590.

[16] H. Elbern, H. Schmidt, A. Ebel, Variational data assimilation for tropospheric chemistry modeling, J. Geophys. Res. 102 (D13) (1997) 15–967.

[17] H. Elbern, H. Schmidt, A. Ebel, Implementation of a parallel 4D-Var chemistry data assimilation scheme, Environ. Management Health 10 (1999) 236–244.

[18] H. Elbern, H. Schmidt, O. Talagrand, A. Ebel, 4D-variational data assimilation with an adjoint air quality model for emission analysis, Environ. Modeling Software 15 (2000) 539–548.

[19] Q. Errera, D. Fonteyn, Four-dimensional variational chemical assimilation of CRISTA stratospheric measurements, J. Geophys. Res. 106 (D11) (2001) 12253–12265.

[20] G. Evensen, Advanced data assimilation for strongly non-linear dynamics, Monthly Weather Rev. 25 (1997) 1342–1354.

[21] M. Fisher, D.J. Lary, Lagrangian four-dimensional variational data assimilation of chemical species, Q.J.R. Meteorol. 121 (1995) 1681–1704.

[22] W.W. Hager, Runge–Kutta methods in optimal control and the transformed adjoint system, Numerische Mathematik 87 (2) (2000) 247–282.

[23] C. Homescu, I.M. Navon, Optimal control of flow with discontinuities, J. Computat. Phys. 187 (2003) 660–682.

[24] D. Lanser, J.G. Verwer, Analysis of operator splitting for advection-diffusion-reaction problems from air pollution modeling, Centrum voor Wiskunde en Informatica Report MAS-R9805, 1998.

[25] A. Hakamiand, M.T. Odman, A.G. Russell, High-order, direct sensitivity analysis of multidimensional air quality models, Environ. Sci. Technol. 37 (11) (2003) 2442–2452.

[26] S. He, G.R. Carmichael, B. Hotchkiss, A. Sandu, V. Damian-Iordache, Application of ADIFOR for air pollution model sensitivity studies, Environ. Modeling Software 15 (2000) 549–557.

[27] P.L. Houtekamer, H.L. Mitchell, Data assimilation using an ensemble Kalman filter technique, Monthly Weather Rev. 126 (3) (1998) 796–811.

[28] W.H. Hundsdorfer, J.G. Verwer, Numerical solution of time-dependent advection-diffusion-reaction equationsSpringer Series in Computational Mathematics, vol. 33, Springer Verlag, Berlin, 2003.

[29] D. Hwang, D.W. Byun, M.T. Odman, An automatic differentiation technique for sensitivity analysis of numerical advection schemes in air quality models, Atmos. Environ. 31 (6) (1997) 879–888.

[30] A.H. Jazwinski, Stochastic Processes and Filtering Theory, Academic Press, New York, 1970.

[31] R.E. Kalman, A new approach to linear filtering and prediction problems, Trans. ASME, Ser. D: J. Basic Eng. 83 (1960) 95–108.

[32] B.V. Khattatov, J.C. Gille, L.V. Lyjak, G.P. Brasseur, V.L. Dvortsov, A.E. Roche, J. Walters, Assimilation of photochemically active species and a case analysis of UARS data, J. Geophys. Res. 104 (1999) 18715–18737.

[33] L. Menut, R. Vautard, M. Beekmann, C. Honor, Sensitivity of photochemical pollution using the adjoint of a simplified chemistry-transport model, J. Geophys. Res. – Atmos. 105-D12 (15) (2000) 15–379.

[34] R. Daley, Atmospheric Data Analysis, Cambridge University Press, London, 1991.

[35] Z. Li, I.M. Navon, Optimality of4D-Var and its relationship with the Kalman filter and Kalman smoother, Q.J.R. Meteorol. Soc. 127 (572 -Part B) (2001) 661–684.

[36] G.I. Marchuk, Adjoint Equations and Analysis of Complex Systems, Kluwer Academic Publishers, Dordrecht, 1995.

[37] G.I. Marchuk, P.V. Agoshkov, I.V. Shutyaev, Adjoint Equations and Perturbation Algorithms in Nonlinear Problems, CRC Press, New York, 1996.

[38] R. Menard, S.E. Cohn, L.-P. Chang, P.M. Lyster, Stratospheric assimilation of chemical tracer observations using a Kalman filter. Part I: Formulation, Monthly Weather Rev. 128 (2000) 2654–2671.

[39] P. Miehe, A. Sandu, G.R. Carmichael, Y. Tang, D. Daescu, A communication library for the parallelization of air quality models on structured grids, Atmos. Environ. 36 (2002) 3917–3930.

[40] R.A. Pielke, W.R. Cotton, R.L. Walko, C.J. Tremback, W.A. Lyons, L.D. Grasso, M.E. Nicholls, M.D. Moran, D.A. Wesley, T.J. Lee, J.H. Copeland, A comprehensive meteorological modeling system – RAMS, Meteorol. Atmos. Phys. 49 (1992) 69–91.

[41] A. Sandu, J.G. Verwer, J.G. Blom, E.J. Spee, G.R. Carmichael, F.A. Potra, Benchmarking stiff ODE solvers for atmospheric chemistry problems II: Rosenbrock methods, Atmos. Environ. 31 (1997) 3459–3472.

[42] A. Sandu, D. Daescu, G.R. Carmichael, Direct and adjoint sensitivity analysis of chemical kinetic systems with KPP: I – theory and software tools, Atmos. Environ. 37 (2003) 5083–5096.

[43] A. Sandu, D. Daescu, Discrete Adjoints for Stiff ODEs, Private communication, 2004.

[44] A. Sei, W. Symes A Note on Consistency and Adjointness of Numerical Schemes. Technical Report CSRPC-TR95527, Center for Research in Parallel Computation, Rice University, January 1995.

[45] Z. Sirkes, E. Tziperman, Finite difference of adjoint or adjoint of finite difference?, Monthly Weather Rev. 49 (1997) 5–40.

[46] B. Sportisse, An analysis of operator splitting techniques in the stiff case, J. Computat. Phys. 161 (2000) 69–91.

[47] R. Vautard, M. Beekmann, L. Menut, Applications of adjoint modeling in atmospheric chemistry: sensitivity and inverse modeling, Environ. Modeling Software 15 (2000) 703–709.

[48] M. van Loon, P.J.H. Builtjes, A.J. Segers, Data assimilation of ozone in the atmospheric transport and chemistry model LOTOS, Environ. Modeling Software 15 (2000) 603–609.

[49] J. Verwer, E.J. Spee, J.G. Blom, W. Hunsdorfer, A second order Rosenbrock method applied to photochemical dispersion problems, SIAM J. Sci. Comput. 20 (1999) 1456–1480.

[50] K.Y. Wang, D.J. Lary, D.E. Shallcross, S.M. Hall, J.A. Pyle, A review on the use of the adjoint method in four-dimensional atmospheric-chemistry data assimilation, Q.J.R. Meteorol. Soc. 127 (576 (Part B)) (2001) 2181–2204.

[51] Y.J. Yang, M.T. Odman, A.G. Russell, Fast three-dimensional sensitivity analysis of photochemical air quality models: an application to southern California, in: Proceedings of the Air and Waste Management Association's Annual Meeting and Exhibition 98-WP76A(06):2, 1998.

[52] Y.J. Yang, J.G. Wilkinson, M.T. Odman, A.G. Russell, Ozone sensitivity and uncertainty analysis using DDM-3D in a photochemical air quality model, Air Pollution Modeling and its Application XIII: Proceedings of the 23rd NATO/CCMS International Technical Meeting on Air Pollution Modelling and Its Application, Varna, Bulgaria:183–194, 2000.